Journal of Catalysis 391 (2020) 282–297

Contents lists available at ScienceDirect

Journal of Catalysis

journal homepage: www.elsevier.com/locate/jcat

Mechanochemical and wet chemical syntheses of CaIn-layered double hydroxide and its performance in a transesterification reaction compared to those of other $Ca_2M(III)$ hydrocalumites (M: Al, Sc, V, Cr, Fe, Ga) and Mg(II)-, Ni(II)-, Co(II)- or Zn(II)-based hydrotalcites

Márton Szabados [a,b], Anna Adél Ádám [a,b], Péter Traj [a,b], Szabolcs Muráth [c,d], Kornélia Baán [e], Péter Bélteky [e], Zoltán Kónya [e,f], Ákos Kukovecz [e], Pál Sipos [b,g], István Pálinkó [a,b,*]

[a] Department of Organic Chemistry, University of Szeged, Dóm tér 8, Szeged H-6720, Hungary
[b] Material and Solution Structure Research Group, Interdisciplinary Excellence Centre, Institute of Chemistry, University of Szeged, Aradi vértanúk tere 1, Szeged H-6720, Hungary
[c] MTA-SZTE Biocolloids Research Group, Rerrich B. tér 1, Szeged H-6720, Hungary
[d] Interdisciplinary Excellence Centre, Department of Physical Chemistry and Materials Science, University of Szeged, Rerrich B. tér 1, Szeged H-6720, Hungary
[e] Department of Applied and Environmental Chemistry, University of Szeged, Rerrich B. tér 1, Szeged H-6720, Hungary
[f] MTA-SZTE Reaction Kinetics and Surface Chemistry Research Group, Rerrich B. tér 1, Szeged H-6720, Hungary
[g] Department of Inorganic and Analytical Chemistry, University of Szeged, Dóm tér 7, Szeged H-6720, Hungary

ARTICLE INFO

Article history:
Received 23 May 2020
Revised 8 July 2020
Accepted 28 July 2020
Available online 2 September 2020

Keywords:
Mechanochemical and wet syntheses of CaIn-LDH
XRD, IR, Raman and DR–UV–Vis spectroscopic characterization
Scanning and transmission electron microscopic studies
Thermal behavior
Transesterification of dimethyl carbonate

ABSTRACT

The feasibility of indium introduction into the hydrocalumite group of layered double hydroxides (LDHs) was investigated for the first time. Mechanochemical and co-precipitation techniques were applied in the syntheses. During the development of preparation, a yet unknown CaIn chloride-hydroxide solid side-product was found and synthesized in phase-pure state. The as-prepared materials were characterized by X-ray diffractometry, Fourier-transform infrared, Raman, and UV–Vis diffuse reflectance spectroscopies. Their thermal behavior was mapped up to 900 °C, while the surface and textural attributes were studied by scanning and transmission electron microscopies, specific surface area measurements and pore size analysis. For the LDH, the $Ca_{2.3}InCl(OH)_{6.6}{\cdot}4H_2O$ and for the side-product, the $Ca_3In_4Cl_2(OH)_{16}{\cdot}6H_2O$ stoichiometric formula was calculated. Various further hydrocalumites (M(III): Al^{3+}, Sc^{3+}, V^{3+}, Cr^{3+}, Fe^{3+}, Ga^{3+}) were synthesized, their surface basicity was investigated by CO_2 temperature programmed desorption. These materials and the indium-containing phases were tested as catalysts in the transesterification reactions of dimethyl carbonate with glycerol. All solids proved to be active: their glycerol conversion capabilities and recycling abilities were determined and compared to the well-known Mg-, Ni-, Co–, Zn-based hydrotalcites.

1. Introduction

Recently, one of the most studied and technologically promising materials are the layered double hydroxides (abbreviated as LDHs and frequently called as hydrotalcite-like materials). Their potential applications spread from the industrial to the healthcare areas; they can serve as anion exchangers, adsorbents in water and flue gas treatments [1–4], polymer additives to achieve fire retardant/resistant character or aid their biological degradation [5], and antacid or drug transporters in medicinal chemistry [6]. However, they receive the most attention as catalysts and/or catalyst supports due to their rich elemental composition. In pristine form, the surface OH^- groups act as Brønsted bases, while after heat treatment at elevated temperatures, the O^{2-} ions are of Lewis base nature. Therefore, the LDHs can promote several base-catalyzed reactions like aldol condensation [7], epoxidation [8], selective N-methylation [9], Michael addition [10], transesterification [11], *etc.*

The formula of $[M(II)_{1-x}M(III)_x(OH)_2]^{x+}[A^{m-}_{x/m}{\cdot}nH_2O)]^{x-}$ describes the composition of most LDHs, where M(II) and M(III) are the di- (Mg^{2+}, Ca^{2+}, Mn^{2+}, Ni^{2+}, Co^{2+}, Cu^{2+}, Zn^{2+} or Cd^{2+}) and trivalent (Al^{3+}, V^{3+}, Cr^{3+}, Fe^{3+}, Co^{3+}, Ga^{3+}) metal ions, respectively, x = M(III)/[M(II) + M(III)] and A^{m-} is for the m-charged changeable interlamellar anions [12]. Their structures are derived from the incorporation of M(III) metal cations (isomorphous substitution of a part of divalent cations) into layered M(II) hydroxide. The positive charge generated

* Corresponding author.
E-mail address: palinko@chem.u-szeged.hu (I. Pálinkó).

https://doi.org/10.1016/j.jcat.2020.07.038
0021-9517/

is compensated by hydrated anions in the interlamellar space, *i.e.* anionic intercalation occurs.

The hydrocalumite group is a member of the hydrotalcite supergroup, where trivalent metal cations are introduced exclusively into the layers of portlandite ($Ca(OH)_2$) isomorphously substituting part of the calcium ions. This framework can be formed only with the fixed x = 0.33 value, due to the heptacoordination (instead of the typical octahedral coordination) of the large-sized Ca(II) [13]. On the seventh apex of Ca-polyhedron, a water molecule or an interlamellar anion is located, and thus the hydrocalumites have increased ion-exchange capabilities [14,15]. The most frequently used and well-probed synthesis way of the hydrocalumites is co-precipitation [15–18]. Recently, the mechanochemical preparation methods have gained significant interest, due to the easily available, simple to set up and moderately priced mills, which allow the synthesis of LDHs with superb quality and occasionally unexpected ratio of metal cations in the layers as well as rare interlayer anions [19,20]. The syntheses of novel hydrocalumites also proved to be feasible in mechanochemically-aided [21] or in pure mechanochemical [22] ways requiring less solvent and less alkaline medium, *i.e.* under greener conditions. Although, the LDH family has members of large variety, the group of hydrocalumites is less populated. While the Al(III) and Fe(III) ions are the most frequent M(III) cations [15–18,21], only a few studies are available with Cr(III)-, Ga(III)- or Sc(III)-containing hydrocalumites [13,23,24].

Although, the occurrence of indium is low in the earth crust, the demand for it has strengthened significantly since the 1990s owing to the intense spread of liquid–crystal displays and solar cells utilizing indium in semiconductor films. Due to the limits of availability, the production, secondary application and recycling of the indium-containing materials start to become highlighted objects nowadays [25,26]. In parallel, studies dealing with the influence of indium species on living organisms also started to gain new impetus. The industrial-scale usage requires careful and increased attention, as for all chemicals, even though they are not considered to be toxic so far [27,28].

Despite the growing interest of the $In(OH)_3$ in photo- and conventional catalytic systems [29–31], indium-containing LDHs were seldom prepared and studied. So far, MgIn-LDH was the major representative made; its structural and thermal features were investigated in detail [32–34], and its catalytic performance in epoxidation [35], transfer hydrogenation [36], benzylation [37] and dehydrogenation reactions [38] also received some attention. In LDH formation, the generally accepted key factor is the difference in ionic radii between the smaller substituting and the larger substituted metal cations [3], and the increase in the ionic radius of M(III) frequently results in decrease in crystallinity [13,39]. Presumably, this is the reason why only sporadic papers deal with the not Mg-based, but ZnIn- and NiIn-LDHs [40,41]. Nevertheless, the large size of Ca(II) ions theoretically allows the incorporation of In(III) cations into the structure of portlandite.

In the last decade, the reduction of the CO_2 emission has become one of the most important goals in the area of transportation. Biodiesel means a renewable alternative to the commonly used fossil sources. It is to be noted, however, that the intensified production resulted in huge glycerol surplus as byproduct of the industrial esterification/transesterification of animal fats or vegetable oils [42–44]. Using this excess is not easy. Fortunately, glycerol is a versatile building bock in many organic molecules. One of the most investigated way of the glycerol conversion is carbonylation with simple dialkyl carbonates or urea due to their low toxicity and high biodegradability [45]. In these reactions, the main products are frequently the highly valuable glycidol (2,3-epoxy-1-propanol), glycerol carbonate (4-hydroxymethyl-1,3-dioxolan-2-one) and their derivatives (diglycerol di- and tricarbonates) [46]. They have industrial potential, for instance, glycidol is a precursor of polymers and medicines [47], glycerol carbonates are used as lubricating oils, surfactants, cosmetics, intermediates of polymers or even electrolytes of Li-ion batteries [48]. Furthermore, glycerol carbonates having high viscosity, water solubility and biodegradability paired with low toxicity and flammability are green and precious platform chemicals [49].

The pristine and the heat-treated layered double hydroxides instantly became popular catalysts for the base-catalyzed transesterification reactions showing excellent performance because of their highly basic character, their improved thermodynamic and structural stabilities compared to the initial metal hydroxide forms and thus, enhanced recycling capability [11,50–53]. While the hydrotalcites are widely tested and improved for transesterification of dimethyl carbonate with glycerol to obtain glycerol carbonate, the work with hydrocalumites remained largely out of scope (limited to the aluminum-containing ones), in spite of the attested outstandingly beneficial presence of the highly basic Ca–OH/Ca–O components in the LDHs [54–56]. In pure form, the calcium oxide and hydroxide phases could be successfully used for glycerol carbonate synthesis; however, they suffered significant deactivation due to the formation of $CaCO_3$ from the water and the carbon dioxide content of the reaction medium/atmosphere and the leaching of calcium as soluble organic species [52,56,57]. In recent studies, the CaAl-LDHs and their calcined derivatives proved to be good alternatives with only slightly lower glycerol conversion capability, but enhanced reusability [52,58–60]. Finally, let us note that LDHs, particularly the hydrocalumites, can be readily produced from the bio- (egg [61], conch [24] shell) and even industrial waste (blast furnace slag [62]).

The aims of the experimental work leading to this contribution were the synthesis of CaIn-LDH, the detailed investigation of its structural, textural, morphological, optical, thermal and basic properties. Furthermore, the CaIn-LDH was applied as catalyst in the transesterification reaction of dimethyl carbonate with glycerol, and compared to the transesterification capabilities of hydrocalumites with various other trivalent cations. Moreover, the potential of the hydrocalumites were further emphasized by the comparative catalytic study of the most frequently prepared members of the hydrotalcites composed of Mg, Ni, Co and Zn divalent and Al, Cr and Fe trivalent metal hydroxides. To the best of our knowledge, there is no report on either the synthesis and characterization of indium-containing hydrocalumites or glycerol transesterification of dimethyl carbonate with glycerol over CaSc-CaV-, CaCr-, CaFe-, CaGa- or CaIn-LDHs.

The results are communicated in the followings.

2. Experimental

2.1. Materials

$CaCl_2{\cdot}2H_2O$, $AlCl_3{\cdot}6H_2O$ $FeCl_3{\cdot}6H_2O$, $CrCl_3{\cdot}6H_2O$, $Ca(OH)_2$ and $InCl_3$ were acquired from Sigma-Aldrich Company (USA). Anhydrous NaOH pellets, $ZnCl_2$, VCl_3, $GaCl_3$, $MgCl_2{\cdot}6H_2O$, $NiCl_2{\cdot}6H_2O$, $CoCl_2{\cdot}6H_2O$ and $ScCl_3{\cdot}6H_2O$ were purchased from VWR International (EU). The indium hydroxide was prepared by the precipitation reaction using 25 wt% aqueous NH_3 solution (from VWR International) and $InCl_3$. The solid was washed by distilled water, and dried for 12 h at 120 °C. All solid materials were of very high purity (99%+).

Glycerol (99.5%) was a VWR product, dimethyl carbonate, dimethyl sulfoxide (DMSO), isopropyl alcohol and *ortho* xylene (all with purities over 99%) were purchased from Sigma-Aldrich.

All chemicals were used as received with no further purification.

2.2. Mechanochemical ways in the synthesis of CaIn-LDH

The first step of mechanical preparations were the co-milling of the starting reagents in a mixer mill (Retsch MM 400) having two grinding jars (stainless steel with 50 cm^3 inner volume) with one grinding ball each (stainless steel with ~ 8.2 cm^3 volume, diameter: 25 mm). The ball/sample mass ratio (60 g/0.6 g), the Ca:In molar ratio (2:1, using anhydrous calcium and indium hydroxide starting materials) and the grinding frequency (12 Hz) were fixed. During the pure mechanochemical method (following a released recipe [22]), the time durations of dry and wet grindings were varied as well as the amount of NaCl solution added. The feasibility of the mechanochemically-aided technique (recipe from [21]) was tested by the systematically modified concentration of added NaCl solution and duration of dry grinding and mechanical stirring in the aqueous environment under inert (N_2) atmosphere and at varying temperatures. At the end of the syntheses, the LDHs prepared were washed several times with distilled water and collected on 0.45 μm filters dried at 90 °C and stored under N_2 atmosphere. N_2 atmosphere was used for all operations.

2.3. The co-precipitation preparation of the layered double hydroxides

The preparation of CaIn-LDH was attempted by mainly following a frequently applied recipe of the co-precipitation synthesis of hydrocalumites in our laboratory [18], where an aqueous mixture of the soluble metal salts is the starting reagent, and base is added to gain the LDHs as precipitates. The calcium and indium chlorides were dissolved in various molar ratios in distilled water (the initial ratio was 2:1–20 cm^3 solution of 0.3 M Ca(II) and 0.15 M In(III) ions). The obtained mixture was fed to 7.1 cm^3 of NaOH aqueous solutions (at varying concentrations) dropwise. The precipitates were stirred mechanically (500 rpm) under N_2 atmosphere at varying temperature and stirring time. Washing, filtering, drying and storing procedures were performed similarly to how was described at the preparation by the mechanochemical method.

In the syntheses of the CaAl-, the CaSc-, the CaV-, the CaCr-, the CaFe- and the CaGa-LDHs, the optimal preparation parameters determined for CaIn-LDH (2 h stirring, 3 M base, room temperature) with 2:1 M(II):M(III) molar ratio were applied, similar conditions proved to be suitable to prepare highly crystalline hydrocalumites with various types of M(III) ions [13,59,63] and even MgAl-, MgIn-LDHs [33,63]. Therefore, these conditions were used for the syntheses of the Mg-, Ni-, Co– and Zn-based hydrotalcites as well, but for the Zn-containing ones only 1.5 M base were applied to avoid the re-dissolution of the zinc hydroxide component. The analytical study of the filter-liquors did not indicate the presence of dissolved metal ions, *i.e.*, all the starting metal reagents were precipitated and showed the typical reflections of LDHs by X-ray diffraction analysis.

2.4. The catalytic transesterification of glycerol

To reveal and study the catalytic potential of the indium-containing hydroxides and compare to those of the other hydrocalumites and hydrotalcites in the transesterification reaction of dimethyl carbonate with glycerol, a solvent-less recipe published in the work of Granados-Reyes *et al.* [52] was used with slight modification. In each test reaction, the applied amounts of the double-distilled glycerol, the catalyst and the dimethyl carbonate were 1.9 g (20.6 mmol), 0.045 g and 6 cm^3 (6.4 g – 71 mmol), respectively, and they were mixed in a glass reactor of 10 cm^3. The reactions were performed under reflux (~90 °C) in air at atmospheric pressure by mechanical stirring (1500 rpm), and the effect of the reaction time was investigated in a wide range (between 2 and 96 h). At the end of the reaction, the obtained mixtures were blended with 2.4 cm^3 of DMSO and purified on 0.45 μm filters. The collected solids were washed with isopropyl alcohol for several times, dried and stored under N_2. The clear liquids were analyzed on a Hewlett-Packard 6890 gas chromatograph equipped with a HP-INNOWax column (30 m × 0.32 mm × 0.5 μm; alternatively, the DB-WAX 52 CB column could also have been used [64,65]) and flame ionization detector. The chromatographic peaks were identified and the glycerol conversion (moles of the converted molecules/moles of the initial glycerol × 100), the selectivity of glycidol and glycerol carbonate (moles of the desired molecules/-moles of the converted glycerol × 100) were determined using commercial calibration standards. The injection (with empty glass insert) and the detector temperature was set at 250 °C, the temperature program started from 70 °C (with 1 min hold), the applied heating rate was 10 °C/min until reaching 210 °C and it continued with 5 °C/min ramp up to 240 °C (with 15 min hold). The injection volume was 0.2 μ l, while *ortho* xylene was used as internal standard.

The role of the DMSO was twofold, as co-solvent aided the dissolution of the unreacted glycerol molecules in the dimethyl carbonate medium, and it also had effect on the separation of the glycidol and glycerol carbonate on the applied column, and helped to determine the selectivity values more precisely (Fig. S1 "S" is the notation used in the Supporting Information). Presumably, the DMSO acted as analyte protectant and modified the various heat-induced degradation of the glycerol carbonate molecules (including to the glycidol as decomposition product as well) [42,43,66] by filling the active sites of the inlet/column [67].

2.5. Methods of structural characterization

The powder X-ray diffractograms (XRD) were registered on a Rigaku Miniflex II instrument, in the Θ = 5–70° range with 4°/min scan speed using $Cu_{K\alpha}$ (λ = 1.5418 Å) radiation. The reflections of normalized diffractograms were assigned by the JCPDS – ICDD (Joint Committee of Powder Diffraction Standards – International Centre for Diffraction Data) database. For calculating the coherently scattering domain sizes of LDH particles (the crystal thicknesses of layers connected to each other), the Scherrer equation with 0.9 shape factor was applied after fitting Gaussian curves on the first reflections. The diffraction pattern of the solids obtained were analyzed using the DICVOL-06 routine included in the Expo2014 package to propose the most probable crystal structures with reflection indexing [68].

The samples were investigated by Fourier-transform infrared (FT-IR) spectroscopy (JASCO FT/IR-4700 spectrophotometer) with 4 cm^{-1} resolution accumulating 256 scans. The spectrometer was equipped with a ZnSe ATR accessory and a DTGS detector. On the normalized curves, the structural properties of the materials were studied in the 4000–650 cm^{-1} wavenumber range.

The FT-Raman spectra were recorded on a Thermo Scientific DXR Raman microscope equipped with a CCD camera and a diode laser. The measurements were performed using the 780 nm laser and at 24 mW power level. The magnification of the optics was 50 × and the aperture of the pinhole was 25 μm. One spectrum was accumulated from 16 scans for 6 s exposure time including fluorescence and cosmic ray corrections. The normalized curves were investigated in the 1200–200 cm^{-1} range.

The morphologies and sizes of the particles prepared were analyzed by scanning (SEM, Hitachi S-4700) and transmission (TEM-FEI TECHNAI G220 X-TWIN instrument) electron microscopies at various magnifications and acceleration voltages. The elemental analysis was performed with energy dispersive X-ray analysis measurements (EDX, Röntec QX2 spectrometer equipped with Be window and coupled to the scanning electron microscope).

The N_2 adsorption–desorption isotherms were recorded on a Quantachrome NOVA 3000e instrument. The materials were degassed at 110 °C for 3 h in vacuum to remove surface-adsorbents. The specific surface areas were calculated by the Brunauer-Emmett-Teller equation from the adsorption branches. To determine the predominant pore sizes and total pore volumes, the Barett-Joyner-Halenda (BJH) method was applied from the desorption branches.

The optical properties of the materials prepared were studied by diffuse reflectance spectroscopy (DRS) with an Ocean Optics USB4000 spectrometer equipped with DH-2000-BAL light source. As white reference, $BaSO_4$ was applied in the 230–800 nm wavelength range. The optical band gaps were estimated from the extrapolation of the straight section of modified Schuster-Kubelka-Munk function plotted vs. energy of incident light.

The thermal behaviors of the samples were characterized by a Setaram Labsys derivatograph working under constant flow of N_2 at 3 °C/min heating rate. For the measurements, 30–35 mg of the solids were placed into high-purity alpha alumina crucibles.

The concentration of calcium and indium ions dissolved in dilute sulfuric acid were measured by a Thermo Scientific iCAP 7400 ICP-OES DUO spectrometer. The ICP Multielement standard solution IV acquired from CertiPUR was applied beside yttrium internal standard.

The basic sites of the materials were mapped by temperature-programmed desorption (TPD) using 99.9% CO_2/He (50 cm^3/min flow). TPD measurements were carried out on a BELCAT-A catalyst analyzer operated with thermal conductivity detector. Before the measurements, ~50 mg of the solids were degassed in He flow and quartz cell at 110 °C for 3 h, after that, the CO_2 saturation were performed at 40 °C. Desorption profiles were recorded up to 800 °C with 10 °C/min heating rate.

3. Results and discussion

3.1. Developing the mechanochemical and co-precipitation types of syntheses for CaIn-LDH

Earlier, it was found that mechanochemical synthesis was only capable to incorporate rarely applied cations (Sn^{4+} and Ti^{4+}) into the layers of portlandite [22,69]. By analogy, the first attempts to prepare CaIn-LDH were performed by mechanochemistry. Mechanochemically-aided and pure mechanochemical techniques were tested varying the synthesis parameters in wide range (Fig. S2-S4). Although the time duration of the wet and the dry milling, the applied temperature and the volume of the added aqueous solution could help (through growing crystal thicknesses) the successful formation of the LDHs (assignation of reflections was based on the CaAl − Cl^--LDH (35–0105) and CaFe − Cl^--LDH (44–0445) JCPDS cards and the work of Rousselot *et al.* [13]), the samples prepared were not phase pure (Fig. 1). Despite our hardest efforts, and the optimal parameters obtained (described in the legend of Fig. 1), signals of unreacted starting reagents $Ca(OH)_2$ (JCPDS#76–0570) and $In(OH)_3$ (JCPDS#76–1464) were always recorded beside the reflections of LDH. Moreover, an unknown secondary phase/side-product was observable, its identification was not successful either on the basis of literature results or the JCPDS database. Measurements performed at a later stage of this study attested the chemical uniformity of this material.

To avoid residues of unreacted starting materials and to understand and inhibit the generation of secondary phase, the preparation of CaIn-LDH was attempted by the co-precipitation method. Firstly, the effect of NaOH concentration on the preparation of the LDH was investigated (Fig. 2). At low concentrations, the generation of hydrocalumite did not occur, solely the reflections of In $(OH)_3$ were observable using 1 M NaOH solution. Increasing the amount of the base added, Ca(II) could precipitate and a new phase appeared referring to as CaIn-hydroxide secondary or side-product in the followings. The reflections of side-product could only be seen on the diffractogram of the sample using 1.5 M base (there were no signs of other secondary products even though others like $Ca(OH)_2$, CaCl(OH), $CaCO_3$, $In(OH)_3$ or InO(OH) could have formed). The further rise in the base concentration increased the amount of the precipitated calcium ions, and, thus, aided the formation of layered double hydroxide, but not exclusively, the reflections of the Ca $(OH)_2$ phase appeared and intensified on increasing the concentration of the base. The crystal thicknesses of LDH particles grew gradually up to the 9 M NaOH solution applied. The optimum base concentration was chosen to be 3 M, where there was no sign of $Ca(OH)_2$ phase.

Since the synthesis of phase-pure CaIn-LDH could not be accomplished by any of the base concentration applied, further investigations were necessary. The effect of time (from 0.5 h to 16 h) and temperature (5–75 °C) of the strring process were studied thoroughly (Fig. S5 and S6). Although the formation of side-product could not be inhibited by the varied reaction parameters, we were capable of tailoring the thicknesses of LDH crystals in wide range, from 14 nm to 31 nm. Interestingly, the determined sizes were systematically lower than those of the substances prepared by the mechanochemical techniques (32–42 nm). Next, the influence of the molar ratios of the starting reagents was studied (Fig. 3). Contrary to the strict 2:1 Ca(II):M(III) cation ratio in the hydrocalumite group, the decrease in the amount of indium resulted in less side-products in smaller amounts. At 2:0.7 Ca:In initial molar ratio, even the most intense reflection of side-product (around 17° 2 θ) was hardly observable, the amount of the side-product became negligible. Further lowering the amount of indium did not result in further improvement, $Ca(OH)_2$ appeared as the third phase. SEM−EDX measurements could identify the molar ratios of the metal ions in the individual particles of the LDH and the side-product. They were close to Ca:In = 2:1 and 1:1 in the hydrocalumite and side-product, respectively. As the summary of the findings, it can be stated that with fixed Ca(II) amount, the decrease in the quantity of In(III) facilitates the formation of phase requiring less indium for the evolution of its crystals. At the initial 2:1.2 Ca:In molar ratio, the enhanced generation of side-product corroborates the above statement. Finally, elemental analysis revealed that both materials contained chlorine; the In:Cl molar ratio was estimated to be 1:1 in the LDHs, while it was 2:1 in the particles of the side-product (from now on it is referred as CaIn-hydroxide-chloride side-product).

3.2. Structural, morphological, textural, optical and thermal characteristics of the CaIn-LDH and the CaIn-hydroxide-chloride side-product

The phase-pure and practically phase-pure syntheses of the side-product and the CaIn-LDH, respectively, allowed us to gain information on their internal structures, surface, optical and thermal properties in detail.

Although, the XRD reflections of the CaIn-LDHs could be identified well with the JCPDS files of the CaAl- and CaFe-LDHs determining the Miller indices of the solids prepared required further investigations using the EXPO2014 crystallographic software package. The LDH was determined to crystallize in a hexagonal structure with $c = 2 \cdot d_0 = 1.559(3)$ nm. The d-spacing value (0.78 nm) was characteristic for the space requirement of chloride anion located in the interlayer gallery [21]. The calculated parameter c was in very good agreement with the one measured by XRD (1.562 nm). In the 5 − 70° 2 θ range, the Miller indices of the major reflections are indicated in Fig. 4. Hexagonal structure was typical

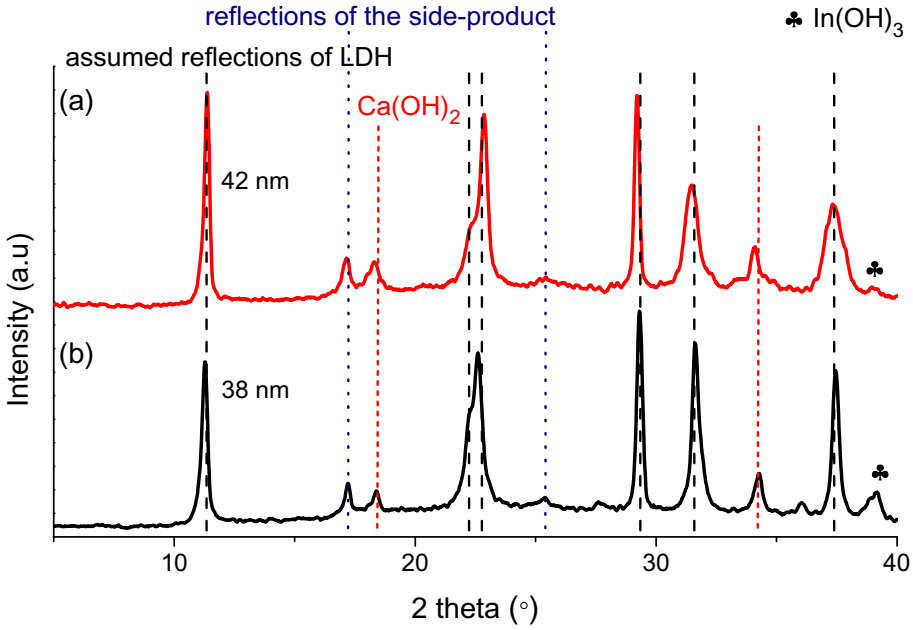

Fig. 1. X-ray powder diffraction patterns of materials prepared with (a) pure mechanochemical (6 h dry and 2 h wet milling, 400 μ l saturated NaCl solution) and (b) mechanochemically-aided (2 h dry grinding, 5 ml 0.4 M NaCl solution, 24 h stirring at 85 °C) syntheses.

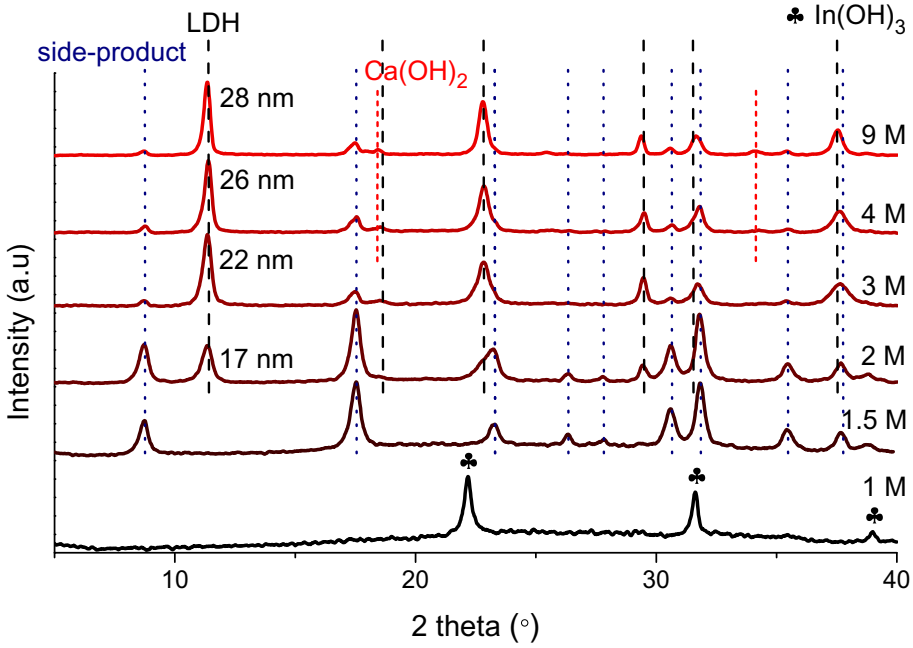

Fig. 2. XRD patterns of the materials prepared with varied base concentrations (room temperature, 2:1 Ca:In molar ratio of starting reagents, 2 h stirring).

for calcium-containing LDHs, the structure of the CaIn-hydroxide-chloride side-product was harder to unfold from XRD results. Two structures seemed plausible; one was the orthorhombic, the other was the monoclinic crystal system. After separate fits, it was found that the orthorhombic system described the structure better. The corresponding Miller indices are shown in Fig. 4, and the relevant data for the possible structures are collected in Table 1. In the orthorhombic structure, 222 class (rhombic disphenoidal) is proposed for the side-product like, for instance, the minerals called adelite $CaMg(AsO_4)(OH)$ or vuagnatite $CaAl(SiO_4)(OH)$.

The structural elements of the as-prepared materials are observed well by FT-IR spectroscopy (Fig. 5). The spectrum of CaIn-LDH shows the characteristic absorption bands of hydrocalumites [68]: the slight shoulder at 3635 cm^{-1} is related to the valence bond stretch of Ca–OH, the wide band with maximum at 3525 cm^{-1} corresponds to the hydroxyl groups in hydrogen bonding network. The bands at 1615 cm^{-1} and 760 cm^{-1} are assigned to the bending vibrations of interlayer water molecules and the OH^- groups, respectively. At 1475 cm^{-1}, the v_3 asymmetric stretching and v_2 bending vibration bands at 870 cm^{-1} of the calcite carbonate group, and the band of the reversibly surface-adsorbed CO_2 molecules at around 1405 cm^{-1} indicates the reaction between the atmospheric CO_2 and the surface Ca–OH molecules. Even though the $CaCO_3$ phase was in undetectable amount for XRD mea-

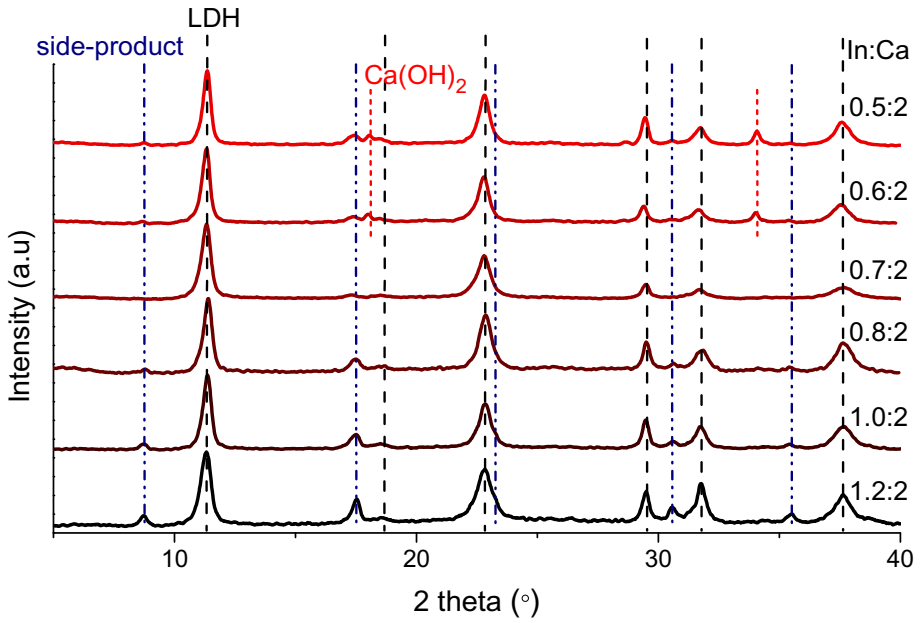

Fig. 3. X-ray powder diffraction patterns for the samples prepared with varying In:Ca molar ratio of the starting reagents (room temperature, 3 M base, 2 h stirring).

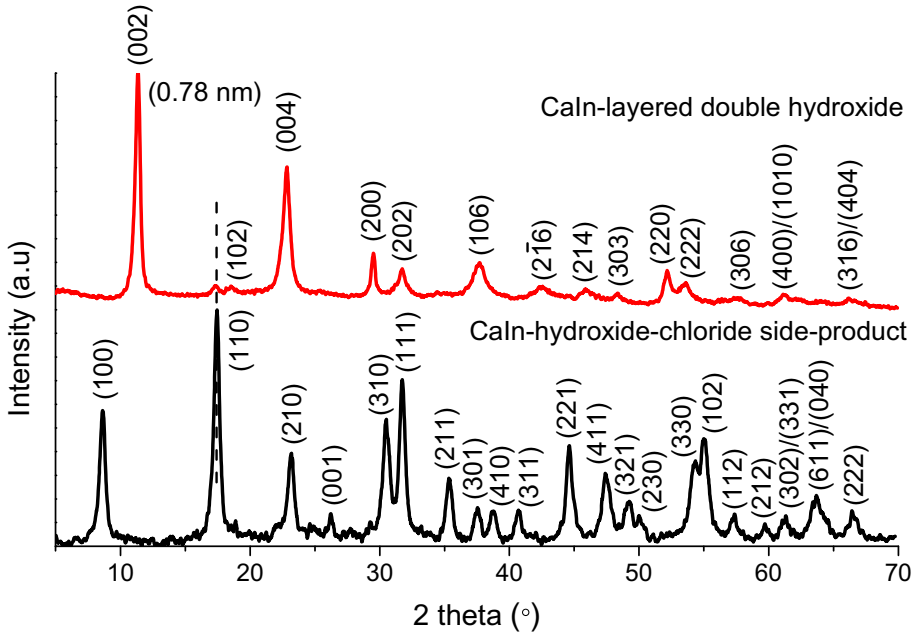

Fig. 4. X-ray powder diffraction patterns of the phase-pure CaIn-hydroxide-chloride side-product (25 °C, 1:2 In:Ca molar ratio of starting reagents, 2 h stirring, 1.5 M base) and the practically phase-pure CaIn-LDH (25 °C, 0.7:2 In:Ca molar ratio, 2 h stirring, 3 M base).

Table 1
Cell parameters of CaIn-LDH and the side-product.

Materials	α, β, γ (°)	a, b, c (nm)	$V_{unit\ cell}$ (nm^3)
CaIn-LDH (hexagonal)	90, 90, 120	0.700, 0.700, 1.559	0.662
CaIn-hydroxide-chloride side-product (orthorhombic)	all 90	1.010, 0.583, 0.338	0.198

surements, it might form during the washing-filtering steps and/or the characterization techniques since preparing, drying, and storing of the samples were performed under N_2 atmosphere.

Several bands of the side-product appeared at similar wavenumbers, but there were significant variations due to the different composition and crystal framework. The position of the band belonging to the stretching vibration of the Ca–OH group did not change; however, its intensity and thus, its visibility was higher. The band corresponding to the hydrogen bonding network of OH^- groups also appeared with 3410 cm^{-1} maximum. The peak belonging to the bending vibration of water molecules was shifted towards higher wavenumber (at 1640 cm^{-1}) indicating that the water molecules were not in the interlayer space, the altered position shows similar local environment to what was recorded for the hydrated $CaCl_2$ salt (Fig. S7). The intensities of the bands of the reversibly adsorbed CO_2 and the *ex situ* generated $CaCO_3$ phase

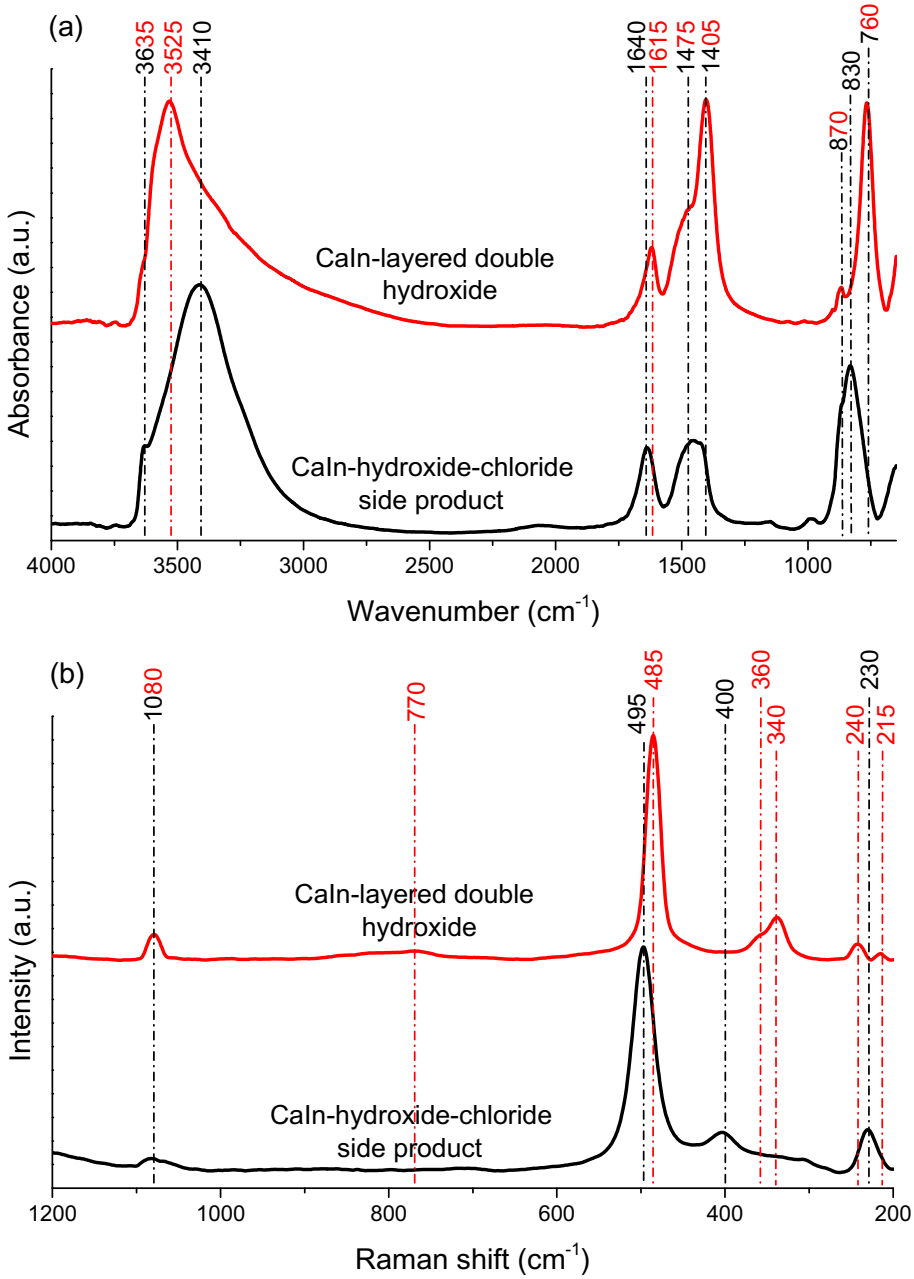

Fig. 5. IR (a) and Raman (b) spectra of the CaIn-hydroxide-chloride side-product and the CaIn-LDH.

decreased owing to the change in the amount of surface Ca–OH groups, because crystals were formed with lower Ca(II) content. Finally, an intense and extended band was found with a maximum at 830 cm^{-1}. This band was merged with those corresponding to the vibrations of $CaCO_3$ (870 cm^{-1}) and the OH^- groups (760 cm^{-1}) mentioned above; however, the maximum may be connected to the vibrations of the O–In–O and In–OH groups [71,72]. The modified character of the Ca–OH and In–OH vibrations indicated that these groups were located more separately than they did in the CaIn-LDH phase.

The Raman spectra of the materials confirmed the structural aspects derived from infrared measurements (Fig. 5). In both cases, the weak signal of the ν_1 CO_3^{2-} stretching mode of calcite phase was observable at 1080 cm^{-1} and the vibration of Ca–O–In coupled with the most intense bands at 485 and 495 cm^{-1} in the LDH and the side-product, respectively [34,70]. The dissimilar position of the bands, related to the lattice vibrational modes of the M – O parts under 400 cm^{-1}, indicated well the significantly different internal structure of the materials prepared. Finally, the broad band around 770 cm^{-1} with small intensity may be attributed to the librational mode of water. The absence of the peaks centered at 680, 710, and 860 cm^{-1} prove that the carbonate as interlayer anion was not present in the CaIn-LDH [73].

The SEM images revealed different morphologies for LDH and the side-product (Fig. 6). The CaIn-LDHs showed distorted hexagonal-shaped particles with lamellar structure. The absence of regular hexagons may be explained by the already mentioned increased size of In(III) cation compared to the M(III) ions in the well-crystallized CaAl- [15] and CaFe-LDHs [74] resulting in decreased crystallinity [13]. SEM images of the side-product attested needle-like morphology, and the particles were closely connected to each other creating few hundred nanometer-long

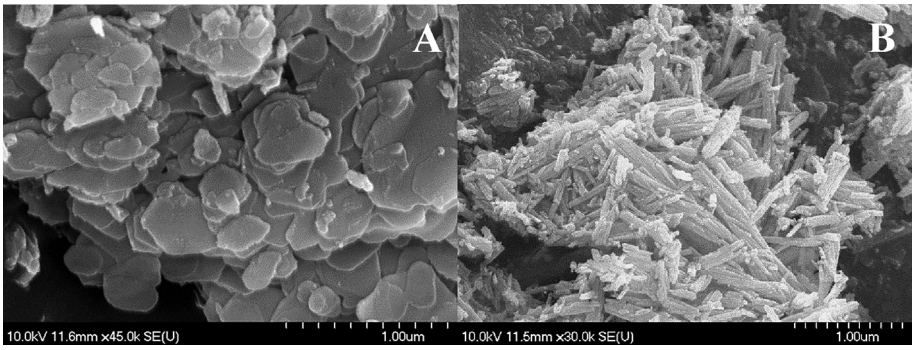

Fig. 6. SEM images of (A) CaIn-LDH and the (B) CaIn-hydroxide-chloride side-product.

fibers. The spatial dimensions of the individual needles were well observable with 300—400 nm length and 20—30 nm width on the TEM images (Fig. 7). Investigations with electron microscopies indicated the chemical uniformity of the side-product: they could not reveal other particles with different morphology, and no segregation of Ca, In or Cl atoms was observed on the elemental map (Fig. S8).

The textural features of the LDH and the side-product had several similarities (Table 4). They showed Type IV isotherms with H3 hysteresis loops according to IUPAC classification (Fig. S9) [75]. They were mesoporous with pore diameters mainly larger than 4 nm, and the LDH had even larger pores (between 10 nm and 50 nm) because of the non-perfect fit among the plate-like hexagonal particles resulting in wedge-shaped pores. The calculated specific surface area and total pore volume were in the range typical for LDHs [76]. Nevertheless, the side-product had higher total pore volume and specific surface area, which was definitely in direct correlation with the long and slim shaped particles.

Since the indium hydroxides/oxides are widely studied as n-type semiconductors, the indium-containing phases prepared were investigated by UV–Vis spectroscopy (Fig. 8), too. The characteristic absorption bands of $In(OH)_3$ (prepared by the addition of 1 M alkali) at around 240 nm and 290 nm were identified [77]. The intensities of the bands were significantly lower in the LDH and the side-product, and a slight blue shift was recorded in the energy gaps in the sequence of the phases prepared. Assuming direct electron band gap transition, the calculated optical energy gaps were 5.20 eV, 5.23 eV, and 5.28 eV for the synthesized $In(OH)_3$, CaIn-hydroxide-chloride side-product, and CaIn-LDH, respectively. The alterations may be related to the decreasing indium hydroxide content and the modification of In−O−In linkages by the incorporated Ca(II) ions.

In the range between 25 and 900 °C, the thermogravimetric and differential thermal analysis (TG−DTA) curves displayed several mass losses for the materials prepared (Fig. 9). The CaIn-LDH sample showed the well-known thermal behavior of LDHs with separated weight losses [76]. In the first step, the physically adsorbed water from the external surface was evaporated under 100 °C in slight amount (1.1% mass loss), then the majority of water molecules (7.5% mass loss) from the interlayer gallery was removed in the 100–180 °C temperature range. Finally, the loss due to the decomposition (*via* dehydroxylation) of the layered metal hydroxides took place at higher temperatures. Presumably, the majority of the hydroxyl groups bound to In departed from 200 to 360 °C, and it was followed by the dehydroxylation of the thermally more stable Ca−OH moieties [21,78].

The CaIn-hydroxide-chloride side-product had some similarities in the positions and intensities of the DTG peaks due to the closely resembling chemical composition. The mass losses at around 105 °C (5.4%) and in the range of 235–270 °C (7.2%) are attributed

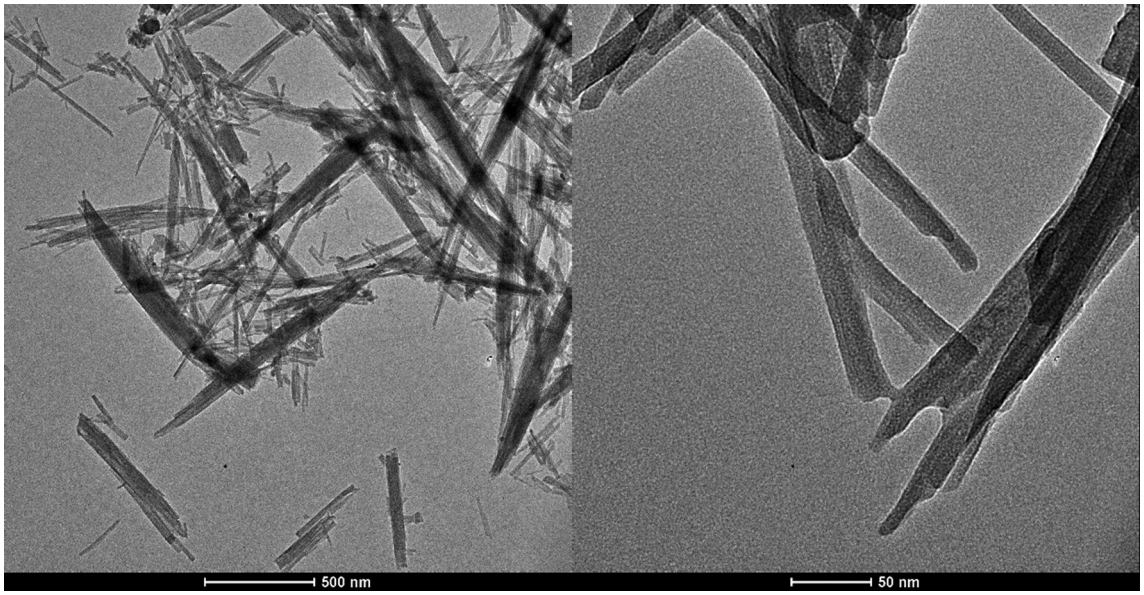

Fig. 7. TEM images of the CaIn-hydroxide-chloride side-product.

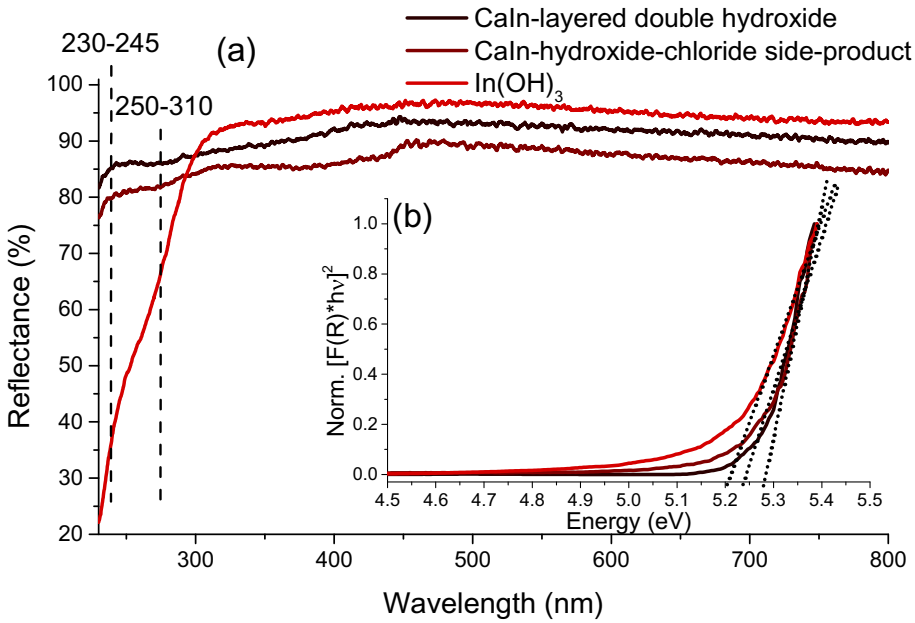

Fig. 8. UV–Vis diffuse reflection spectra (a) and Tauc plot (b) of the materials CaIn-LDH, CaIn-hydroxide-chloride side-product and $In(OH)_3$.

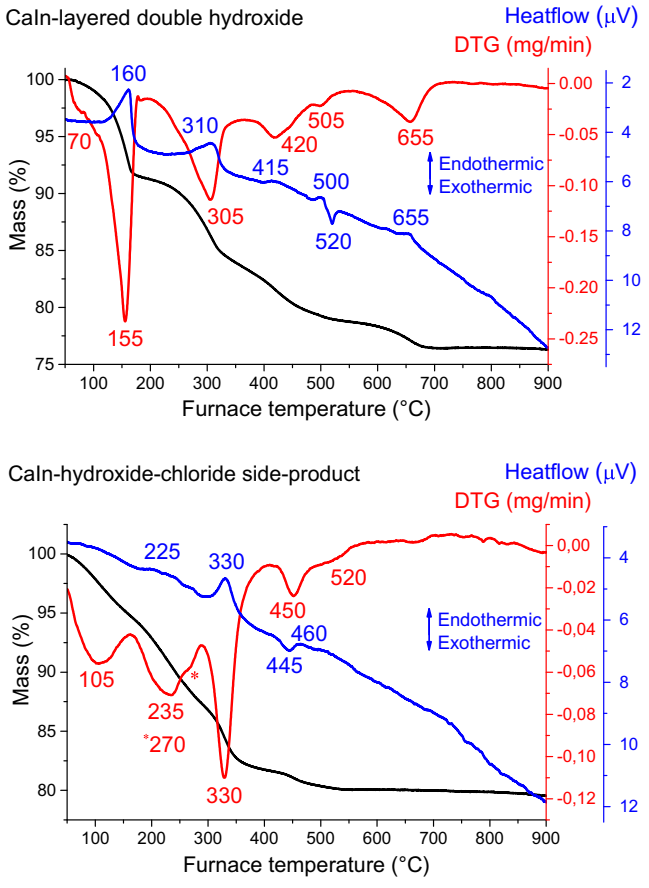

Fig. 9. Thermal analysis curves of the samples CaIn-LDH, CaIn-hydroxide-chloride side-product.

partially to the removal of physisorbed water molecules and mainly to crystal water. From 290 °C, the dehydroxylation of the metal hydroxides started with gradually decreasing weight loss values at higher temperatures. The DTG peaks at 330 °C and 450 °C maxima indicated 5.6% and 1.2% mass losses, while the final step around 520 °C resulted in negligible (0.5%) weight decrease. Interestingly, the total weight loss values of the LDH and the side-product were smaller than it was expected from the SEM–EDX elemental ratio calculations, and unusual chemical compositions could also be estimated from the ICP analysis of the materials heat-treated at 900 °C. The XRD measurements displayed reflections related to $CaIn_2O_4$ (JCPDS#17–0643) and CaO (JCPDS#82–1691) phases in the heat-treated samples (Fig. S10), and SEM–EDX analysis showed the presence of chlorine as well. The observed anomalies can be interpreted well by assuming that the chloride anions were oxidized to Cl^{3+} and/or Cl^{5+} cations. In addition, the above-discussed DTG peaks were exclusively connected to endothermic processes; however, the DTA curves showed exothermic peaks for the CaIn-LDH (at 520 °C) and the CaIn-hydroxide-chloride side-product (at 445 °C) as well. These peaks may be connected to the formation of oxidized chloride [79] containing amorphous calcium and/or indium oxide phases, and give explanation for the reduced mass losses (1% – 505 °C and 1.2% – 450 °C).

Data from the SEM–EDX measurements, the TG curves and the ICP analyses together give detailed information on the chemical composition of the hydroxides prepared. The stoichiometric formulas suggested are the followings; $Ca_{2.3}InCl(OH)_{6.6}{\cdot}4H_2O$ for the LDH and $Ca_3In_4Cl_2(OH)_{16}{\cdot}6H_2O$ for the side-product (it is referred as Ca_3In_4 side-product as well). For the increased Ca:In molar ratio (slightly higher than the mentioned strict 2:1 ratio typical for hydrocalumites) can be explained by the formation of amorphous $Ca(OH)_2$ side-product and/or the decreased indium incorporation into the LDH structure. It has been published in several reports that the increased radius of the M(III) ion had negative effect on the efficiency of cation incorporation into the M(II) hydroxide layers resulting in decreased crystallinity [13,39,80,81]. Let us point out that the obtained optimal Ca:In ratio was higher (greater than2.8:1) than it was established in the layers of the LDH when it was prepared in a practically phase-pure state, which indicated that during the washing procedure, the main part of the slaked lime could be removed due to its enhanced dissolution compared to the thermodynamically more stable LDH phase [50,82].

3.3. Catalytic transesterification tests for the CaIn-LDH and the Ca_3In_4-hydroxide-chloride side-product

Both indium-containing solids proved to be active catalysts in the transesterification of the dimethyl carbonate with the glycerol molecules (without catalyst the conversion of the glycerol was under 7% after 24 h). The primary transformation pathway was the transesterification reaction producing glycerol carbonate (Fig. 10).

This product, then reacted further in three channels. Glycidol was formed, through the decarboxylation of the glycerol carbonate, presumably on the stronger basic sites [43,64], and just slightly from the dehydration of glycerol: its yield was under 1% after 6 h reaction time. This observation coincides well with that experienced over MgAl-LDH [83] (Fig. 11/a). Diglycerol dicarbonate was formed from the dehydration of two glycerol carbonate molecules (Fig. 11/b). Diglycerol tricarbonate, also using two glycerol carbonate and one dimethyl carbonate molecules, is transesterification product (Fig. 11/c), and this was the least significant secondary reaction.

The results of a representative measurements of this complex consecutive reaction system are given in Table 2 consisting of the glycerol carbonate derivatives and the residual glycerol in mmols. Note that the sum of glycerol carbonate derivative products and the unreacted glycerol accounts for the glycerol introduced meaning that there was no other reaction in the system.

For CaIn-LDH, the conversions of glycerol (Table 3) were relatively high in the first six hours; however, they were significantly lower over the Ca_3In_4 side-product. To reach similar conversion levels required significantly more time.

3.4. Comparative catalytic and reusability studies

To compare the catalytic potential of CaIn-LDH to those of other hydrocalumites, CaAl-, CaSc-, CaV-, CaCr-, CaFe- and CaGa-LDHs were synthesized under the same conditions (but with fixed 2:1 M(II):M(III) molar ratio) as the CaIn-LDH was made, and tested in transesterification. In every case, the SEM–EDX analysis verified the presence of the Ca:M(III):Cl ions with around 2:1:1 M ratio, while the XRD (Fig. S11) and IR (Fig. S12) measurements showed the typical signals of the LDHs without any contaminant phases (save for the weak adsorption band of the calcite), but with varied crystal thicknesses (between 6 and 32 nm). The diffuse reflection spectrum of the CaV-LDH displayed an absorption band around

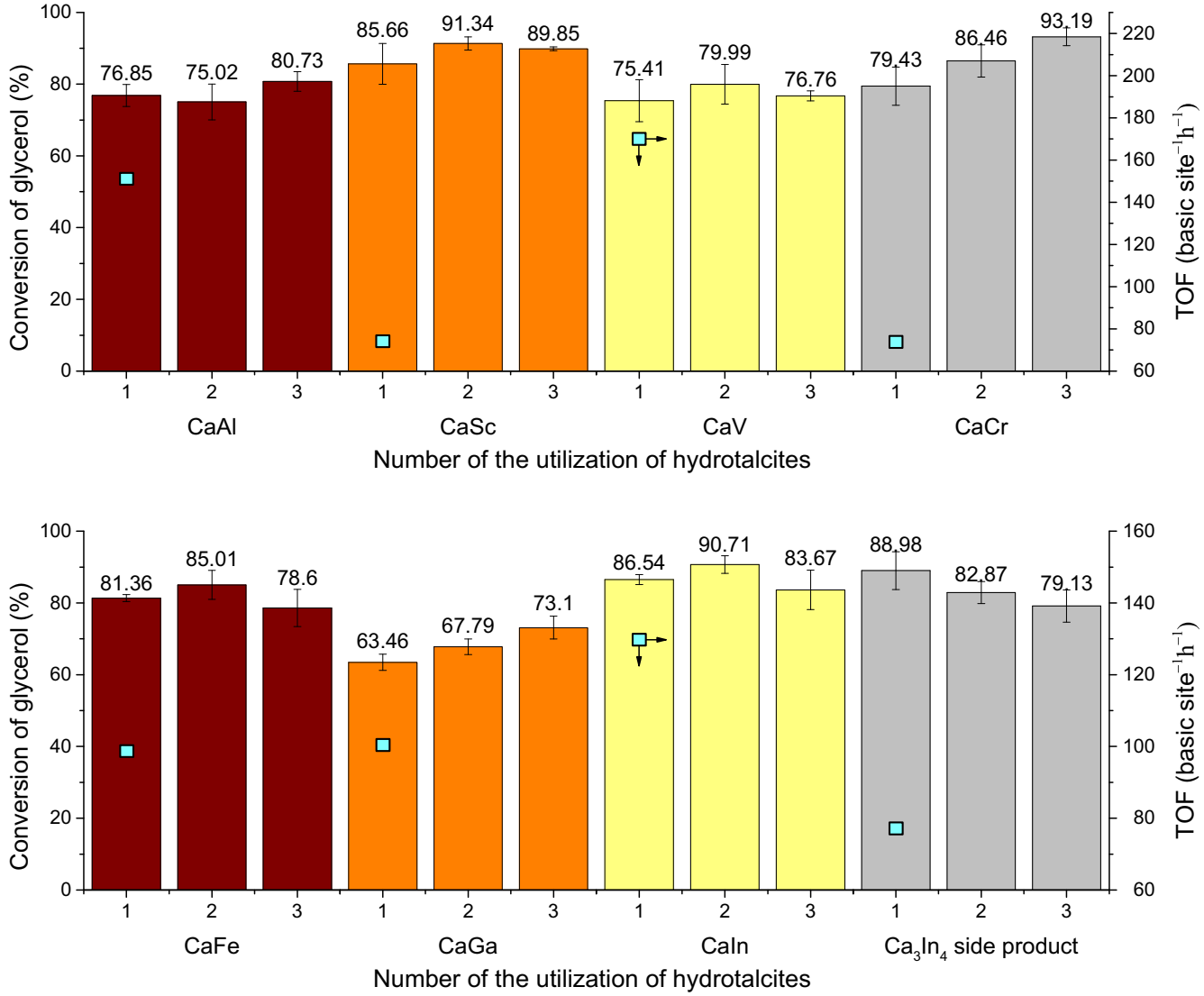

Fig. 10. Catalytic and reusability tests of the hydrocalumites (6 h reaction time) and Ca_3In_4-hydroxide-chloride side-product (72 h reaction time), reaction conditions: reflux (~90 °C), glycerol 20.6 mmol, dimethyl carbonate 71 mmol, catalyst 45 mg, stirring 1500 rpm, air atmosphere; □ – TOF values for the first uses (for details, see also Table 4 and the corresponding text).

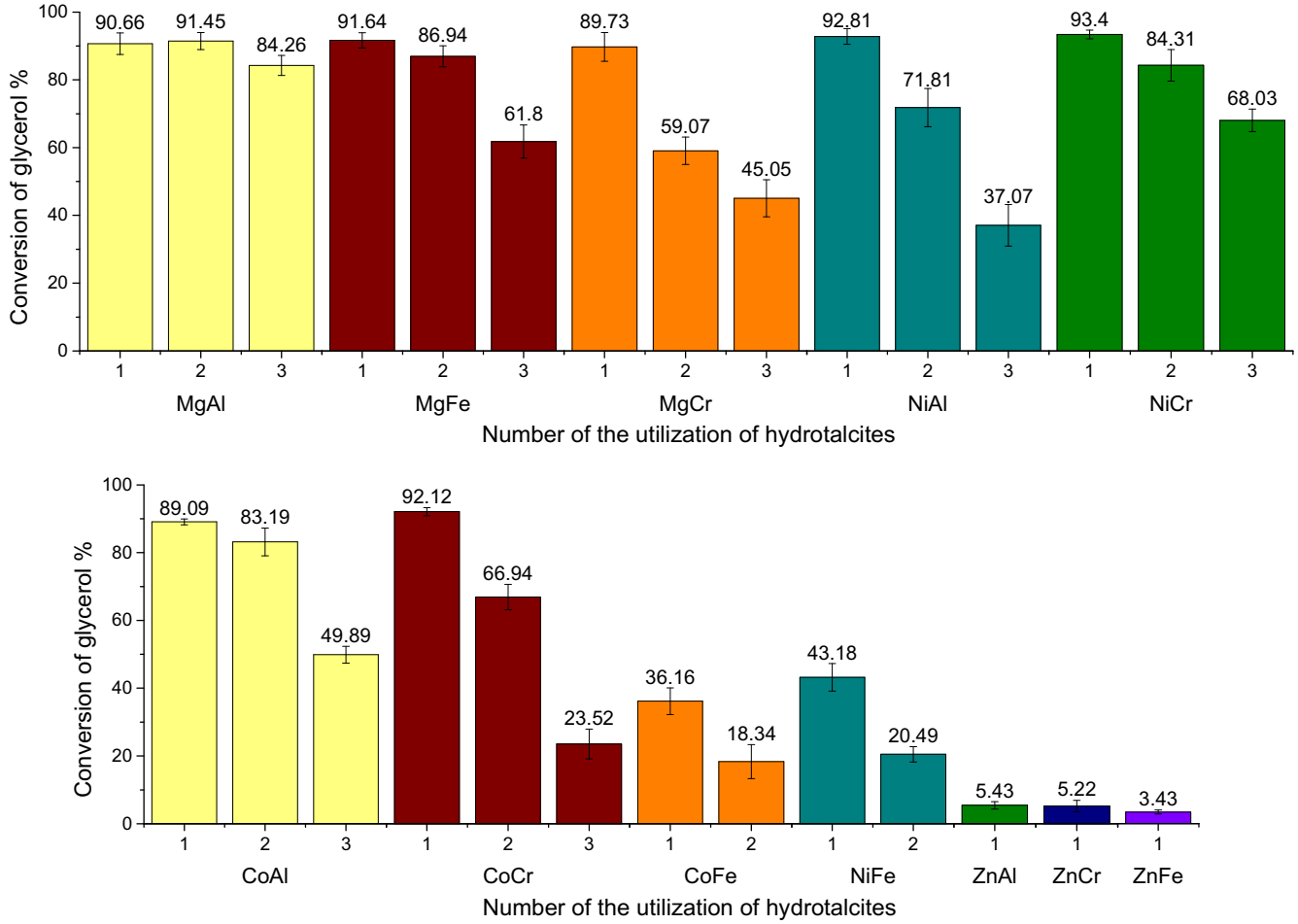

Fig. 11. Glycerol conversion over various hydrotalcites, reaction conditions: reflux (~90 °C), glycerol 20.6 mmol, dimethyl carbonate 71 mmol, catalyst 45 mg, stirring 1500 rpm, air atmosphere, 6 h.

Table 2
The quantities of glycerol carbonate derivatives and the residual glycerol in mmol over the In-containing materials at various reaction times.

Reaction time (h)	Glycerol(mmol)	Glycerol carbonate (mmol)	Glycidol(mmol)	Diglycerol decarbonate (mmol)	Diglycerol tricarbonate (mmol)
CaIn-LDH					
2	9.11	8.84	1.73	0.46	0
4	5.89	11.19	1.79	0.70	0.17
4 (N_2 atmosphere)	5.83	10.75	2.10	0.71	0.25
6	2.78	12.24	2.25	1.20	0.47
8	2.45	12.71	1.92	1.25	0.51
12	2.45	12.63	1.90	1.23	0.58
16	1.92	12.55	1.98	1.46	0.62
24	1.13	12.46	1.98	1.67	0.86
Ca_3In_4 side-product					
16	17.10	2.60	0.68	0.11	0
24	14.67	4.47	1.30	0.08	0
48	11.91	6.37	1.90	0.21	0
60	8.20	8.71	2.50	0.56	0.04
72	2.27	11.87	2.93	1.23	0.54
96	1.32	11.21	3.36	1.48	0.88

Reaction conditions: reflux (~90 °C), glycerol 20.6 mmol, dimethyl carbonate 71 mmol, catalyst 45 mg, stirring 1500 rpm, air atmosphere (except the test with CaIn-LDH

600 nm indicating the successful incorporation and preservation of the air sensitive V^{3+} cations in the calcium hydroxide environment beside the ligand–metal charge transfer transitions of the V^{5+} (~400 nm), presumably located on or near the surface of the layers (Fig. S13) [84,85].

All members of the hydrocalumites showed appreciable glycerol conversion (63–86%) on first use (Scheme 1). During the second and third uses, the rates of glycerol conversion were very well maintained. The recycling tests of the Ca_3In_4 side-product resulted in similar results with slight decrease in glycerol conversion (Scheme 1). In spite of the relatively stable catalytic performance, several structural and quality changes were observed by XRD measurements (Fig. S11): the hydrocalumites gradually lost their layered framework (*via* the continuous reduction in the crys-

Table 3
Conversions of glycerol over the In-containing materials (CaIn-LDH and Ca_3In_4 side-product in glycerol transesterification (reaction conditions: reflux (~90 °C), glycerol 20.6 mmol, dimethyl carbonate 71 mmol, catalyst 45 mg, stirring 1500 rpm, air, except one reaction over CaIn-LDH).

CaIn-LDH	Conversion of glycerol	Ca_3In_4 side-product	Conversion of glycerol
reaction time of 2 h	55.83 ± 4.24	reaction time of 16 h	17.13 ± 3.4
4 h	71.45 ± 2.95	24 h	28.76 ± 5.09
4 h N_2 atm.	71.67 ± 2.02	48 h	42.18 ± 5.0
6 h	86.54 ± 1.39	60 h	60.17 ± 4.13
8 h	88.07 ± 0.76	72 h	88.98 ± 5.09
12 h	88.13 ± 0.61	96 h	93.63 ± 1.85
16 h	90.74 ± 1.34		
24 h	94.51 ± 3.9		

tal thicknesses) during the repeated transesterifications. The stabilities of CaSc-, and CaIn-LDHs were the highest, their first reflections around 11° 2θ were observable even after the second and third uses, but the X-ray diffractograms of the others indicated the intensified evolution of amorphous states. Interestingly, there were no signs of $CaCO_3$ formation; however, unidentified reflections were observed for the CaV-LDH. The CaIn-LDH and the Ca_3In_4 side-product attested different behavior, the structural integrity of the side-product proved to be higher than those of the hydrocalumites, and even the CaIn-LDHs could slowly transform into the phase of Ca_3In_4-hydroxide-chloride. Finally, the XRD patterns revealed another well-known side effect of the co-solvent dimethyl sulfoxide: it aided the delamination of the layers as it was demonstrated for the CaAl-LDH as well. Delamination, counterbalancing the gradual loss of the layered structure, could be responsible for the stable and occasionally slightly promoted glycerol conversion *via* enhancing the accessible surface of the hydroxides explaining the slightly different reuse behavior of the side-product with more robust framework.

Infrared spectroscopy measurements revealed the elevated formation of calcite phase (~1490 cm^{-1}) and physisorbed CO_2 except for the Ca_3In_4 side-product, where significantly weaker signals were only observed (Fig. S12). For the CaV-LDH used three times, these vibrations also lost intensity, probably connected to the evolution of a new and unidentified phase. Beside the C–H vibrations around 2900 cm^{-1}, the C=O, asymmetric and symmetric C–O stretching (around 1780, 1100 and 1045 cm^{-1}, respectively) verified the presence of retained glycerol carbonate [86] merged with the characteristic absorption bands of the hydroxide phases. The surface-adsorbed glycerol could not be ruled out either, due to the strong stretching absorption of the C–O groups located at the around 1110 (linkage in C2) and 1040 cm^{-1} (C1 and C3), too [87]. The SEM−EDX records decreasing quantities of calcium and chloride: the Ca:M(III):Cl molar ratio became 1.7–1.1:1:0.3–0.04 after the third application of the LDHs, while sulfur from DMSO residue was not detected. The reduction in chloride quantity was remarkably high implying an active anion-exchange process during the transesterification, presumably with other charge-compensating species like hydroxide or even glyceroxide ions. For the Ca_3In_4 side-product, leaching of the calcium and chloride ions were also recorded in similar extent.

3.5. Interpretation of the catalytic results

To provide a more appropriate description of the catalytic results, detailed specific surface, textural and basicity investigations were performed. The findings are detailed in the followings.

All hydrocalumites roughly showed type IV isotherms with H3 hysteresis (Fig. S9), and the measured predominant pore sizes were similar to that of CaIn-LDH. However, the specific surface areas and

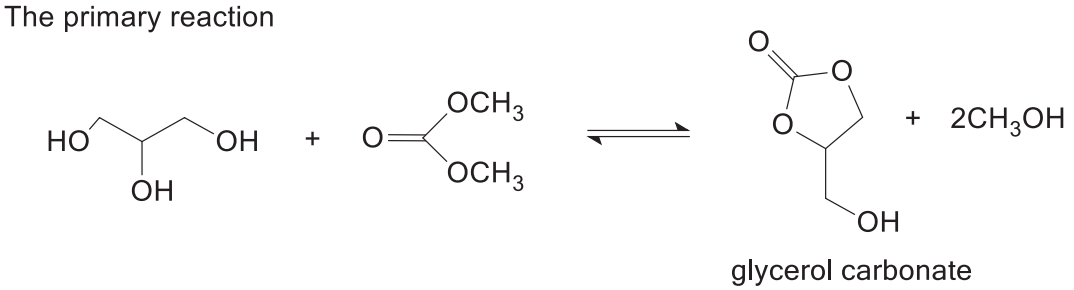

Scheme 1. Transesterification of dimethyl carbonate with glycerol over the In-containing materials and the other LDHs of this study.

Table 4
Textural, activity and basicity parameters of the hydrocalumite samples and the side-product.

Materials	Specific surface area (m^2/g)	Total pore volume (cm^3/g)	Predominant pore size diameters (nm)	Total basic sites (μmol/g)	TOF[a] (basic site$^{-1}h^{-1}$)
CaAl-LDH	14.0	0.026	3.1	390	151
CaSc-LDH	69.3	0.188	3.8, 11.4–30.8	890	73.6
CaV-LDH	19.6	0.032	3.2	340	169
CaCr-LDH	29.3	0.111	3.9, 11.2–23.3	830	73.1
CaFe-LDH	20.3	0.065	3.3, 17.4–30.4	630	98.7
CaGa-LDH	6.7	0.018	3.3	480	101
CaIn-LDH	34.8	0.120	3.9, 9.7–46.7	510	130
Ca_3In_4 side-product	82.5	0.179	3.6	220	77.3[b]

Reaction conditions: reflux (~90 °C), glycerol 20.6 mmol, dimethyl carbonate 71 mmol, catalyst 45 mg, stirring 1500 rpm, air atmosphere
[a] The conversion values observed over the as-prepared samples after 6 h reaction time were used.
[b] The conversion value after 24 h reaction time was used.

the total pore volume values changed in a wide range(Table 4, columns 2 and 3).

It is known that transesterification is catalyzed by basic sites, therefore CO_2 temperature programmed desorption measurements were performed in order to determine the quality as well as the quantities of the basic sites on our hydrocalumite samples, and the In-containing side-product. Since the pristine forms of our samples included strongly bonded CO_2 molecules as surface carbonates and even as interlayer CO_3^{2-} anions in varied amount, blank measurements were performed to take into account the amount of CO_2 originating from the desorption of these moieties. The TPD spectra obtained (Fig. S14) were divided to three regions as weak (50–200/250 °C), moderate (250–500 °C) and strong (above 500 °C) basic sites. The basicity values obtained were comparable to calcined MgAl-LDHs [65] and to those of Zheng [58], López-Salinas [88] and Rossi *et al.* [89] recorded for the mildly heat-treated and pristine CaAl-LDHs, and the estimated total basicities were normalized to the mass (Table 4, column 4) of the catalyst samples and reaction rates (turnover frequency – TOF in basic site^{-1}h^{-1}) were calculated on the basis of total basicity (Table 4, column 5). It is assumed that the activated complex uses all the basic sites available to CO_2. There is good chance that this approximation is accurate enough, since the majority of the LDHs are mesoporous, therefore basic sites even in the inside of the agglomerates as well as among the layers are accessible for the reactants as well. It is seen that there are no dramatic differences in the activities of the various hydrocalumites, and the novel CaIn-LDH belongs to the top three performers. The In-containing side-product had also remarkable activity, higher than CaSc- and CaCr-LDHs, but with lowest basicity, presumably due to the lower Ca:M(III) molar ratio in the stoichiometric formula and thus the lower number of the more basic Ca—OH parts on the external surface. Moreover, the distribution of the basic sites showed large difference, the amount of the weak sites were more than 35% of the total basic sites, while this was between 8 and 20% for the hydrocalumites, except the 30% for the CaV-LDHs (might be induced by the presence of V^{5+} species). These observations are parallel with those of the findings by Takagaki *et al.*, namely the moderately strong sites could be the main active species of the LDHs [90], and might explain the required longer reaction times for the Ca_3In_4 side-product.

Finally, to demonstrate the promising catalytic potential of the hydrocalumites, additional experiments were performed using the most frequently prepared and studied hydrotalcites with M(II) =

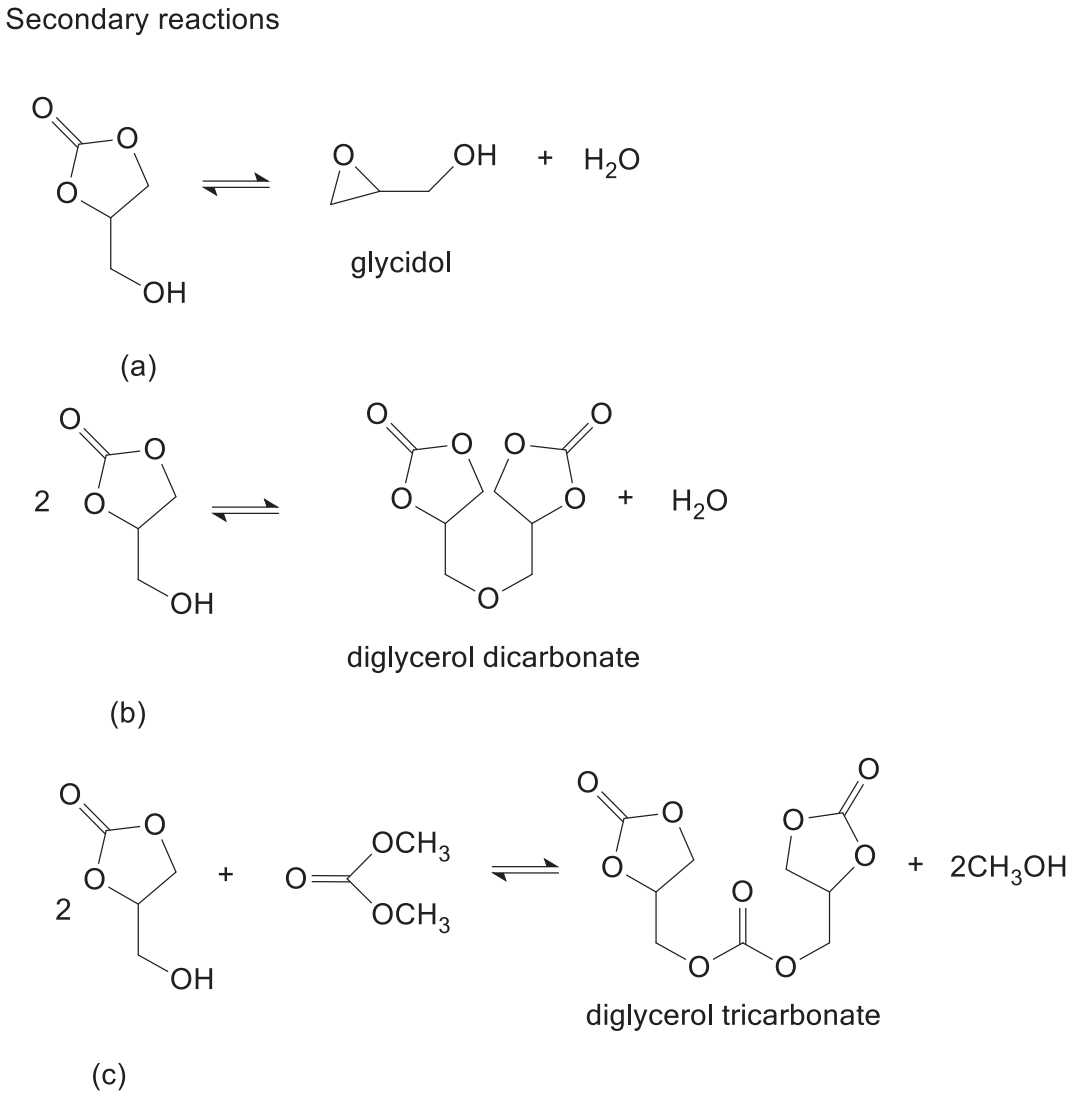

Scheme 2. Secondary transformation pathways occurring over the In-containing materials and the other LDHs of this study.

(Mg^{2+}, Ni^{2+}, Co^{2+}, Zn^{2+}) and M(III) = (Al^{3+}, Cr^{3+}, Fe^{3+}) (Fig. 11). They were strictly synthesized with the already used parameters of the co-precipitation method (2:1 M(II):M(III) molar ratio, 2 h mechanical stirring at room temperature), and the crystal thicknesses were mainly under (3–12 nm) those of the ones determined for the hydrocalumites accompanied by lower specific surface values (between 1.2 and 6 m^2/g) as well (Fig. S15). Interestingly, and somewhat surprisingly, the NiFe-, CoFe- and the Zn-containing LDHs acted very poorly in their freshly prepared states, but the performances of the as-prepared MgAl-, MgFe-, MgCr-, NiAl-, NiCr-, CoAl- and CoCr-LDHs were similar to those of the hydrocalumites (Fig. 11). However, the obtained selectivity values of the glycerol carbonate productions were slightly higher over the Ni- and Co-based solids, the recycling ability of MgAl-LDH was only comparable. During the reuse tests, the hydrotalcites suffered significantly faster deactivation, in spite of the similar gradual amorphization of the layered framework (Fig. S15). Although the observations for series of Mg_2Al- and Mg_5Al-LDHs [90], a direct correlation between the crystal thicknesses of the hydrocalumites/hydrotalcites and the values of glycerol conversion could not be observed, and even after the largely uniform structural amorphization of the solids, the obtained catalytic results of the hydrotalcites were still remarkably different. However, it seems that all hydrocalumites performed significantly better, their reuse potential was less dependent on the chemical quality of the M(III) hydroxide components in the layers, probably due to the predominance of the Ca–OH moiety, which has highly polarized basicity determining bond.

4. Conclusions

CaIn-layered double hydroxide was successfully prepared by mechanochemical and the co-precipitation techniques together with a previously unknown Ca-In-chloride-hydroxide secondary product. The infrared, Raman, and UV–Vis diffuse reflectance spectroscopies recorded several similar structural attributes for the two phases; however, indexing the reflections in the X-ray powder patterns revealed that the LDH had hexagonal, while the side-product had orthorhombic or monoclinic crystal system. The electron microscopic images showed needle-like morphology for the Ca-In-chloride-hydroxide secondary product.

In transesterification reactions, the catalytic potential of the indium-containing phases were investigated and compared to the common (CaAl-, CaFe-LDHs), the rarely investigated CaSc-, CaCr-, CaGa-LDHs and the new CaV-LDH. These hydrocalumite LDH samples were highly active in the transesterification reaction of dimethyl carbonate with glycerol. They also put out appreciable recycling abilities. The Ca-In-chloride-hydroxide side-product had comparable activity, and also performed well in the reuse tests. Among the many hydrotalcites tested under the same conditions in the same reaction, only the performance of MgAl-LDH was comparable to the hydrocalumite solids. The experimental data obtained verified that the hydrocalumites could be economically friendly, bio-based and easily accessible/producible and hence promising alternatives of the hydrotalcites in glycerol transesterification, and perhaps in other base-catalyzed reactions.

Declaration of Competing Interest

None.

Acknowledgement

This work was supported by the European Union and the Hungarian government through grant GINOP-2.3.2-15- 2016-00013. The financial help is highly appreciated.

Appendix A. Supplementary material

Supplementary data to this article can be found online at https://doi.org/10.1016/j.jcat.2020.07.038.

References

[1] Y. Seida, Y. Nakano, Removal of phosphate by layered double hydroxides containing iron, Water Res. 36 (5) (2002) 1306–1312, https://doi.org/10.1016/S0043-1354(01)00340-2.
[2] F.L. Theiss, G.A. Ayoko, R.L. Frost, Removal of boron species by layered double hydroxides: A review, J. Colloid Interface Sci. 402 (2013) 114–121, https://doi.org/10.1016/j.jcis.2013.03.051.
[3] A. Corma, A.E. Palomares, F. Rey, F. Márquez, Simultaneous Catalytic Removal of SOxand NOxwith Hydrotalcite-Derived Mixed Oxides Containing Copper, and Their Possibilities to Be Used in FCC Units, J. Catal. 170 (1) (1997) 140–149, https://doi.org/10.1006/jcat.1997.1750.
[4] Y. Ding, E. Alpay, High Temperature Recovery of CO_2 from Flue Gases Using Hydrotalcite Adsorbent, Process Saf. Environ. Prot. 79 (1) (2001) 45–51, https://doi.org/10.1205/095758201531130.
[5] S. Sinha Ray, M. Okamoto, Polymer/layered silicate nanocomposites: a review from preparation to processing, Prog. Polym. Sci. 28 (11) (2003) 1539–1641, https://doi.org/10.1016/j.progpolymsci.2003.08.002.
[6] C. Delhoyo, Layered double hydroxides and human health: An overview✠, Appl. Clay Sci. 36 (1-3) (2007) 103–121, https://doi.org/10.1016/j.clay.2006.06.010.
[7] D. Tichit, M. Naciri Bennani, F. Figueras, R. Tessier, J. Kervennal, Aldol condensation of acetone over layered double hydroxides of the meixnerite type, Appl. Clay Sci. 13 (5-6) (1998) 401–415, https://doi.org/10.1016/S0169-1317(98)00035-0.
[8] S. Ueno, K. Yoshida, K. Ebitani, K. Kaneda, Hydrotalcite catalysis: heterogeneous epoxidation of olefins using hydrogen peroxide in the presence of nitriles, Chem. Commun. (1998) 295–296. https://doi.org/10.1039/A707655J
[9] J. Santhanalakshmi, T. Raja, Selective N-methylation of aniline by calcined MgIIAlIII layered double hydroxides, Appl. Catal. A 147 (1) (1996) 69–80, https://doi.org/10.1016/S0926-860X(96)00190-1.
[10] B.M. Choudary, M. Lakshmi Kantam, C.R. Venkat Reddy, K. Koteswara Rao, F. Figueras, The first example of Michael addition catalysed by modified Mg–Al hydrotalcite, J. Mol. Catal. A: Chem. 146 (1-2) (1999) 279–284, https://doi.org/10.1016/S1381-1169(99)00099-0.
[11] B.M. Choudary, M.L. Kantam, C.V. Reddy, S. Aranganathan, P.L. Santhi, F. Figueras, Mg–Al–O–t-Bu hydrotalcite: a new and efficient heterogeneous catalyst for transesterification, J. Mol. Catal. A Chem. 159 (2000) 411–416, https://doi.org/10.1016/S1381-1169(00)00209-0.
[12] G.D. Evans, R.C.T. Slade, Structural aspects of layered double hydroxides, Struct. Bond. 119 (2006) 1–87, https://doi.org/10.1007/430_005.
[13] I. Rousselot, C. Taviot-Guého, F. Leroux, P. Léone, P. Palvadeau, J.-P. Besse, Insights on the Structural Chemistry of Hydrocalumite and Hydrotalcite-like Materials: Investigation of the Series $Ca_2M^{3+}(OH)_6Cl{\cdot}2H_2O$ (M^{3+}: Al^{3+}, Ga^{3+}, Fe^{3+}, and Sc^{3+}) by X-Ray Powder Diffraction, J. Solid State Chem. 167 (1) (2002) 137–144, https://doi.org/10.1006/jssc.2002.9635.
[14] G. Renaudin, M. Francois, O. Evrard, Order and disorder in the lamellar hydrated tetracalcium monocarboaluminate compound, Cem. Concr. Res. 29 (1) (1999) 63–69, https://doi.org/10.1016/S0008-8846(98)00184-7.
[15] Y. Chen, Z. Shui, W. Chen, G. Chen, Chloride binding of synthetic Ca–Al–NO_3 LDHs in hardened cement paste, Constr. Build. Mater. 93 (2015) 1051–1058, https://doi.org/10.1016/j.conbuildmat.2015.05.047.
[16] I. Dékány, T. Haraszti, Layered solid particles as self-assembled films, Colloids Surf., A 123-124 (1997) 391–401, https://doi.org/10.1016/S0927-7757(96)03804-6.
[17] M. Park, C.-I. Lee, E.-J. Lee, J.-H. Choy, J.-E. Kim, J. Choi, Layered double hydroxides as potential solid base for beneficial remediation of endosulfan-contaminated soils, J. Phys. Chem. Solids 65 (2-3) (2004) 513–516, https://doi.org/10.1016/j.jpcs.2003.09.022.
[18] V. Bugris, M. Ádok-Sipiczki, T. Anitics, E. Kuzmann, Z. Homonnay, Á. Kukovecz, Z. Kónya, P. Sipos, I. Pálinkó, Thermal decomposition and reconstruction of CaFe-layered double hydroxide studied by X-ray diffractometry and ^{57}Fe Mössbauer spectroscopy, J. Mol. Struct. 1090 (2015) 19–24, https://doi.org/10.1016/j.molstruc.2014.10.039.
[19] G.R. Williams, S.J. Moorhouse, T.J. Prior, A.M. Fogg, N.H. Rees, D. O'Hare, New insights into the intercalation chemistry of $Al(OH)_3$, Dalton Trans. 40 (22) (2011) 6012, https://doi.org/10.1039/c0dt01790F.
[20] S.(. Intasa-ard, K.(. Imwiset, S. Bureekaew, M. Ogawa, Mechanochemical methods for the preparation of intercalation compounds, from intercalation to the formation of layered double hydroxides, Dalton Trans. 47 (9) (2018) 2896–2916, https://doi.org/10.1039/C7DT03736H.
[21] M. Szabados, K. Pásztor, Z. Csendes, S. Muráth, Z. Kónya, Á. Kukovecz, S. Carlson, P. Sipos, I. Pálinkó, Synthesis of high-quality, well-characterized CaAlFe-layered triple hydroxide with the combination of dry-milling and ultrasonic irradiation in aqueous solution at elevated temperature, Ultrason. Sonochem. 32 (2016) 173–180, https://doi.org/10.1016/j.ultsonch.2016.03.008.

[22] Z. Ferencz, M. Szabados, M. Ádok-Sipiczki, Á. Kukovecz, Z. Kónya, P. Sipos, I. Pálinkó, Mechanochemically assisted synthesis of pristine Ca(II)Sn(IV)-layered double hydroxides and their amino acid intercalated nanocomposites, J. Mater. Sci. 49 (24) (2014) 8478–8486, https://doi.org/10.1007/s10853-014-8558-8.
[23] R. Allmann, Doppelschichtstrukturen mit brucitähnlichen Schichtionen [Me(II)$_{1-x}$Me(III)$_x$(OH)$_2$]$^{x+}$, Chimia 24 (1970) 99–108.
[24] R.O.A. Adelagun, N.A. Oladoja, I.A. Ololade, A.S. Adeyemo, Evaluation of layered double hydroxide synthesised from a green biogenic precursor for phosphate removal: characterisations and isotherms, Am. J. Biosci. 5 (2017) 13–24. https://doi.org/10.11648/j.ajbio.20170502.11.
[25] M. Frenzel, C. Mikolajczak, M.A. Reuter, J. Gutzmer, Quantifying the relative availability of high-tech by-product metals – The cases of gallium, germanium and indium, Resour. Policy 52 (2017) 327–335, https://doi.org/10.1016/j.resourpol.2017.04.008.
[26] C.J. Rhodes, Endangered elements, critical raw materials and conflict minerals, Sci. Prog. 102 (4) (2019) 304–350, https://doi.org/10.1177/0036850419884873.
[27] C.J. Hines, J.L. Roberts, R.N. Andrews, M.V. Jackson, J.A. Deddens, Use of and Occupational Exposure to Indium in the United States, J. Occup. Environ. Hygiene 10 (12) (2013) 723–733, https://doi.org/10.1080/15459624.2013.836279.
[28] S.J.O. White, J.P. Shine, Exposure Potential and Health Impacts of Indium and Gallium, Metals Critical to Emerging Electronics and Energy Technologies, Curr. Envir. Health Rpt 3 (4) (2016) 459–467, https://doi.org/10.1007/s40572-016-0118-8.
[29] Y. Onishi, D. Ogawa, M. Yasuda, A. Baba, Direct Conversion of carbonyl compounds into organic halides: Indium(III) hydroxide-catalyzed deoxygenative halogenation using chlorodimethylsilane, J. Am. Chem. Soc. 124 (2002) 13690–13691, https://doi.org/10.1021/ja0283246.
[30] T. Yan, J. Long, Y. Chen, X. Wang, D. Li, X. Fu, Indium hydroxide: A highly active and low deactivated catalyst for photoinduced oxidation of benzene, C. R. Chim. 11 (1-2) (2008) 101–106, https://doi.org/10.1016/j.crci.2007.02.012.
[31] Y. Li, Y. Hou, Q. Fu, S. Peng, Y.H. Hu, Oriented growth of ZnIn2S4/In(OH)3 heterojunction by a facile hydrothermal transformation for efficient photocatalytic H2 production, Appl. Catal. B 206 (2017) 726–733, https://doi.org/10.1016/j.apcatb.2017.01.062.
[32] M.A. Aramendía, V. Borau, C. Jiménez, J.M. Marinas, J.M. Luque, J.R. Ruiz, F.J. Urbano, Synthesis and characterization of a novel Mg/In hydrotalcite-like compound, Mater. Lett. 43 (3) (2000) 118–121, https://doi.org/10.1016/S0167-577X(99)00243-8.
[33] R.L. Frost, S.J. Palmer, L.-M. Grand, Synthesis and thermal analysis of indium-based hydrotalcites of formula $Mg_6In_2(CO_3)(OH)_{16}{\cdot}4H_2O$, J. Therm. Anal. Calorim. 101 (3) (2010) 859–863, https://doi.org/10.1007/s10973-009-0439-z.
[34] R.L. Frost, S.J. Palmer, L.-M. Grand, Synthesis and Raman spectroscopy of indium-based hydrotalcites of formula $Mg_6In_2(CO_3)(OH)_{16}{\cdot}\ 4_H2O$, J. Raman Spectrosc. 41 (12) (2010) 1797–1802, https://doi.org/10.1002/jrs.2571.
[35] M.A. Aramendia, V. Borau, C. Jimenez, J.M. Luque, J.M. Marinas, F.J. Romero, J.R. Ruiz, F.J. Urbano, Epoxidation of limonene with layered-double hydroxides as catalysts, Stud. Surf. Sci. Catal. 130 (2000) 1667–1672, https://doi.org/10.1016/S0167-2991(00)80440-1.
[36] M.A. Aramendia, V. Borau, C. Jimenez, J.M. Marinas, F.J. Romero, J.R. Ruiz, F.J. Urbano, Catalytic transfer hydrogenation of citral on calcined layered double hydroxides, Appl. Catal. A-Gen. 206 (2001) 95–101, https://doi.org/10.1016/S0926-860X(00)00588-3.
[37] V.R. Choudhary, R. Jha, V.S. Narkhede, In-Mg-hydrotalcite anionic clay as catalyst or catalyst precursor for Friedel–Crafts type benzylation reactions, J. Mol. Catal. A: Chem. 239 (1-2) (2005) 76–81, https://doi.org/10.1016/j.molcata.2005.06.003.
[38] M. Gabrovska, R. Edreva-Kardjieva, V. Angelov, D. Crisan, G. Muteanu, J. Védrine, Mg-Al and Mg-In oxide compounds as catalyst components for the oxidative dehydrogenation of propane. Part I, Rev. Roum. Chim. 52 (2007) 521–525.
[39] M.A. Aramendia, V. Borau, C. Jimenez, J.M. Marinas, J.R. Ruiz, F.J. Urbano, Comparative study of Mg/M(III) (M=Al, Ga, In) layered double hydroxides obtained by coprecipitation and the sol–gel method, J. Solid State Chem. 168 (2002) 156–161, https://doi.org/10.1006/jssc.2002.9655.
[40] X. Liu, Q. Shao, Y. Zhang, X. Wang, J. Lin, Y. Gan, M. Dong, Z. Guo, Microwave hydrothermal synthesized ZnIn-layered double hydroxides derived ZnIn-layered double oxides for enhanced methylene blue photodegradation, Colloids Surf., A 592 (2020) 124588, https://doi.org/10.1016/j.colsurfa.2020.124588.
[41] K. Teramura, S. Iguchi, Y. Mizuno, T. Shishido, T. Tanaka, Photocatalytic Conversion of CO_2 in Water over Layered Double Hydroxides, Angew. Chem. Int. Ed. 51 (32) (2012) 8008–8011, https://doi.org/10.1002/anie.201201847.
[42] M.O. Sonnati, S. Amigoni, E.P. Taffin de Givenchy, T. Darmanin, O. Choulet, F. Guittard, Glycerol carbonate as a versatile building block for tomorrow: synthesis, reactivity, properties and applications, Green Chem. 15 (2) (2013) 283–306, https://doi.org/10.1039/C2GC36525A.
[43] M. Szőri, B.R. Giri, Z. Wang, A.E. Dawood, B. Viskolcz, A. Farooq, Glycerol carbonate as a fuel additive for a sustainable future, Sustain. Energy Fuels 2 (10) (2018) 2171–2178, https://doi.org/10.1039/c8se00207j.
[44] P. Caro, M. Bandres, M. Urrutigoïty, C. Cecutti, S. Thiebaud-Roux, Recent progress in synthesis of glycerol carbonate and evaluation of its plasticizing properties, Front. Chem. 7 (2019) 308, https://doi.org/10.3389/fchem.2019.00308.
[45] P. Tundo, M. Musolino, F. Aricò, The reactions of dimethyl carbonate and its derivatives, Green Chem. 20 (1) (2018) 28–85, https://doi.org/10.1039/C7GC01764B.
[46] M. Aresta, A. Dibenedetto, L. di Bitonto, New efficient and recyclable catalysts for the synthesis of di- and tri-glycerol carbonates, RSC Adv. 5 (79) (2015) 64433–64443, https://doi.org/10.1039/C5RA06981E.
[47] A. Fajdek, A. Wróblewska, E. Milchert, Significance and use of glycidol, Chemik 64 (2010) 362–375.
[48] A. Rodrigues, J.C. Bordado, R.G. dos Santos, Upgrading the glycerol from biodiesel production as a source of energy carriers and chemicals—A technological review for three chemical pathways, Energies 10 (2017) 1817. https://doi.org/10.3390/en10111817.
[49] J.R. Ochoa-Gómez, O. Gómez-Jiménez-Aberasturi, C. Ramírez-López, M. Belsué, A Brief Review on Industrial Alternatives for the Manufacturing of Glycerol Carbonate, a Green Chemical, Org. Process Res. Dev. 16 (3) (2012) 389–399, https://doi.org/10.1021/op200369v.
[50] C.A. Johnson, F.P. Glasser, Hydrotalcite-like minerals (M2Al(OH)6(CO3)0.5.× H2O, where M = Mg, Zn Co, Ni) in the environment: synthesis, characterization and thermodynamic stability, Clays Clay Miner. 51 (2003) 1–8, https://doi.org/10.1346/CCMN.2003.510101.
[51] G. Fan, F. Li, D.G. Evans, X. Duan, Catalytic applications of layered double hydroxides: recent advances and perspectives, Chem. Soc. Rev. 43 (20) (2014) 7040–7066, https://doi.org/10.1039/C4CS00160E.
[52] J. Granados-Reyes, P. Salagre, Y. Cesteros, CaAl-layered double hydroxides as active catalysts for the transesterification of glycerol to glycerol carbonate, Appl. Clay Sci. 132-133 (2016) 216–222, https://doi.org/10.1016/j.clay.2016.06.008.
[53] G. Arrabito, A. Bonasera, G. Prestopino, A. Orsini, A. Mattoccia, E. Martinelli, B. Pignataro, P.G. Medaglia, Layered double hydroxides: A toolbox for chemistry and biology, Crystals 9 (2019) 361. https://doi.org/10.3390/cryst9070361.
[54] I. Cota, E. Ramírez, F. Medina, J.E. Sueiras, G. Layrac, D. Tichit, New synthesis route of hydrocalumite-type materials and their application as basic catalysts for aldol condensation, Appl. Clay Sci. 50 (4) (2010) 498–502, https://doi.org/10.1016/j.clay.2010.09.019.
[55] Y. Liao, F. Li, X. Dai, N. Zhao, F. Xiao, Solid base catalysts derived from Ca-M-Al (M = Mg, La, Ce, Y) layered double hydroxides for dimethyl carbonate synthesis by transesterification of methanol with propylene carbonate, Chin. J. Catal. 38 (11) (2017) 1860–1869, https://doi.org/10.1016/S1872-2067(17)62898-5.
[56] S. Kondawar, C. Rode, Solvent-Free Glycerol Transesterification with Propylene Carbonate to Glycerol Carbonate over a Solid Base Catalyst, Energy Fuels 31 (4) (2017) 4361–4371, https://doi.org/10.1021/acs.energyfuels.7b00034.
[57] J.R. Ochoa-Gómez, O. Gómez-Jiménez-Aberasturi, B. Maestro-Madurga, A. Pesquera-Rodríguez, C. Ramírez-López, L. Lorenzo-Ibarreta, J. Torrecilla-Soria, M.C. Villarán-Velasco, Synthesis of glycerol carbonate from glycerol and dimethyl carbonate by transesterification: Catalyst screening and reaction optimization, Appl. Catal. A 366 (2) (2009) 315–324, https://doi.org/10.1016/j.apcata.2009.07.020.
[58] L. Zheng, S. Xia, X. Lu, Z. Hou, Transesterification of glycerol with dimethyl carbonate over calcined Ca-Al hydrocalumite, Chin. J. Catal. 36 (10) (2015) 1759–1765, https://doi.org/10.1016/S1872-2067(15)60915-9.
[59] J. Granados-Reyes, P. Salagre, Y. Cesteros, Effect of the preparation conditions on the catalytic activity of calcined Ca/Al-layered double hydroxides for the synthesis of glycerol carbonate, Appl. Catal. A 536 (2017) 9–17, https://doi.org/10.1016/j.apcata.2017.02.013.
[60] J. Granados-Reyes, P. Salagre, Y. Cesteros, Boosted selectivity towards glycerol carbonate using microwaves vs conventional heating for the catalytic transesterification of glycerol, Appl. Clay Sci. 156 (2018) 110–115, https://doi.org/10.1016/j.clay.2018.01.025.
[61] Y. Kuwahara, T. Ohmichi, T. Kamegawa, K. Mori, H. Yamashita, A novel conversion process for waste slag: synthesis of a hydrotalcite-like compound and zeolite from blast furnace slag and evaluation of adsorption capacities, J. Mater. Chem. 20 (24) (2010) 5052, https://doi.org/10.1039/c0jm00518e.
[62] S. Li, F. Wang, X. Jing, J. Wang, J. Saba, Q.i. Liu, L. Ge, D. Song, M. Zhang, Synthesis of layered double hydroxides from eggshells, Mater. Chem. Phys. 132 (1) (2012) 39–43, https://doi.org/10.1016/j.matchemphys.2011.10.049.
[63] S. Muráth, M. Szabados, D. Sebők, Á. Kukovecz, Z. Kónya, I. Szilágyi, P. Sipos, I. Pálinkó, Influencing the texture and morphological properties of layered double hydroxides with the most diluted solvent mixtures – The effect of 6–8 carbon alcohols and temperature, Colloids Surf., A 574 (2019) 146–153, https://doi.org/10.1016/j.colsurfa.2019.04.053.
[64] S. Pan, L. Zheng, R. Nie, S. Xia, P. Chen, Z. Hou, Transesterification of Glycerol with Dimethyl Carbonate to Glycerol Carbonate over Na–based Zeolites, Chin. J. Catal. 33 (11-12) (2012) 1772–1777, https://doi.org/10.1016/S1872-2067(11)60450-6.
[65] L. Zheng, S. Xia, Z. Hou, M. Zhang, Z. Hou, Chinese, J. Catal. 35 (2014) 310–318, https://doi.org/10.1016/S1872-2067(12)60738-4.
[66] H.A. Bruson, T.W. Riener, Thermal decomposition of glyceryl carbonates, J. Am. Chem. Soc. 74 (1952) 2100–2101. https://doi.org/10.1021/ja01128a504.
[67] M. Anastassiades, K. Maštovská, S.J. Lehotay, Evaluation of analyte protectants to improve gas chromatographic analysis of pesticides, J. Chromatogr. A 1015 (1-2) (2003) 163–184, https://doi.org/10.1016/S0021-9673(03)01208-1.
[68] A. Altomare, C. Cuocci, C. Giacovazzo, A. Moliterni, R. Rizzi, N. Corriero, A. Falcicchio, EXPO2013: a kit of tools for phasing crystal structures from powder data, J. Appl. Crystallogr. 46 (4) (2013) 1231–1235, https://doi.org/10.1107/S0021889813013113.

[69] J. Qu, L. Sha, Z. Xu, Z. He, M. Wu, C. Wu, Q. Zhang, Calcium chloride addition to overcome the barriers for synthesizing new Ca-Ti layered double hydroxide by mechanochemistry, Appl. Clay Sci. 173 (2019) 29–34, https://doi.org/10.1016/j.clay.2019.02.017.
[70] M. Al-Jaberi, S. Naille, M. Dossot, C. Ruby, Interlayer interaction in Ca–Fe layered double hydroxides intercalated with nitrate and chloride species, J. Mol. Struct. 1102 (2015) 253–260, https://doi.org/10.1016/j.molstruc.2015.08.064.
[71] J. Yang, H. Cheng, W.N. Martens, R.L. Frost, Application of infrared emission spectroscopy to the thermal transition of indium hydroxide to indium oxide nanocubes, Appl. Spectrosc. 65 (2011) 113–118. https://doi.org/10.1366/10-06082
[72] S. Dhanasingh, D. Nallasamy, S. Padmanapan, V.C. Padaki, Cetyltrimethylammonium bromide- and ethylene glycol-assisted preparation of mono-dispersed indium oxide nanoparticles using hydrothermal method, Chem. Pap. 68 (2014) 1079–1086, https://doi.org/10.2478/s11696-014-0543-9.
[73] R.L. Frost, S.J. Palmer, F. Theiss, Synthesis and Raman spectroscopic characterisation of hydrotalcites based on the formula Ca 6 Al 2 (CO 3)(OH) 16 · 4H 2 O, J. Raman Spectrosc. 42 (5) (2011) 1163–1167, https://doi.org/10.1002/jrs.2827.
[74] P. Sipos, I. Pálinkó, As-prepared and intercalated layered double hydroxides of the hydrocalumite type as efficient catalysts in various reactions, Catal. Today 306 (2018) 32–41, https://doi.org/10.1016/j.cattod.2016.12.004.
[75] K.S.W. Sing, D.H. Everett, R.A.W. Hall, L. Moscou, R.A. Pierotti, J. Rouquérol, T. Siemieniewska, Reporting physisorption data for gas/solid systems with special reference to the determination of surface area and porosity, Pure Appl. Chem. 57 (1985) 603–619, https://doi.org/10.1351/pac198557040603.
[76] C. Forano, T. Hibino, F. Leroux, C. Taviot-Guého, Layered double hydroxides, Develop. Clay Sci. 1 (2006) 1021–1095, https://doi.org/10.1016/S1572-4352(05)01039-1.
[77] S. Avivi, Y. Mastai, A. Gedanken, Sonohydrolysis of In^{3+} ions: Formation of needle like particles of indium hydroxide, Chem. Mater. 12 (2000) 1229–1233, https://doi.org/10.1021/cm9903677.
[78] T. Sato, Preparation and thermal decomposition of indium hydroxide, J. Therm. Anal. Calorim. 82 (3) (2005) 775–782, https://doi.org/10.1007/s10973-005-0963-4.
[79] A.E. Newkirk, D.W. McKee, Thermal decomposition of rhodium, iridium, and ruthenium chlorides, J. Catal. 11 (1968) 370–377, https://doi.org/10.1016/0021-9517(68)90061-4.
[80] J.M. Fernández, C. Barriga, M.A. Ulibarri, F.M. Labajos, V. Rives, New Hydrotalcite-like Compounds Containing Yttrium, Chem. Mater. 9 (1) (1997) 312–318, https://doi.org/10.1021/cm9603720.
[81] C.X. Chen, Y. Zhang, H.Q. Zhao, J.S. Peng, B. Li, Preparation and characterization of nanocrystalline Ce-containing layered double hydroxides, Adv. Mat. Res. 239−242 (2011) 375−379. https://doi.org/10.4028/www.scientific.net/AMR.239-242.375.
[82] M. Szabados, A.A. Ádám, Z. Kónya, Á. Kukovecz, S. Carlson, P. Sipos, I. Pálinkó, Effects of ultrasonic irradiation on the synthesis, crystallization, thermal and dissolution behaviour of chloride-intercalated, co-precipitated CaFe-layered double hydroxide, Ultrason. Sonochem. 55 (2019) 165–173, https://doi.org/10.1016/j.ultsonch.2019.02.024.
[83] Z. Liu, J. Wang, M. Kang, N. Yin, X. Wang, Y. Tan, Y. Zhu, Structure-activity correlations of LiNO 3 /Mg 4 AlO 5.5 catalysts for glycerol carbonate synthesis from glycerol and dimethyl carbonate, J. Ind. Eng. Chem. 21 (2015) 394–399, https://doi.org/10.1016/j.jiec.2014.02.051.
[84] L.J. Burcham, G. Deo, X. Gao, I.E. Wachs, In situ IR, Raman, and UV-Vis DRS spectroscopy of supported vanadium oxide catalysts during methanol oxidation, Top. Catal. 11 (2000) 85–100, https://doi.org/10.1023/A:1027275225668.
[85] N.H. Choi, S.-K. Kwon, H. Kim, Analysis of the Oxidation of the V(II) by Dissolved Oxygen Using UV-Visible Spectrophotometry in a Vanadium Redox Flow Battery, J. Electrochem. Soc. 160 (6) (2013) A973–A979, https://doi.org/10.1149/2.145306jes.
[86] V. Calvino-Casilda, G. Mul, J.F. Fernández, F. Rubio-Marcos, M.A. Bañares, Monitoring the catalytic synthesis of glycerol carbonate by real-time attenuated total reflection FTIR spectroscopy, Appl. Catal. A 409-410 (2011) 106–112, https://doi.org/10.1016/j.apcata.2011.09.036.
[87] P. Guerrero, A. Retegi, N. Gabilondo, K. de la Caba, Mechanical and thermal properties of soy protein films processed by casting and compression, J. Food Eng. 100 (1) (2010) 145–151, https://doi.org/10.1016/j.jfoodeng.2010.03.039.
[88] E. Lopez-Salinas, M.E.L. Serrano, M.A.C. Jácome, I.S. Secora, Characterization of synthetic hydrocalumite-type $[Ca_2Al(OH)_6]NO_3.mH_20$: Effect of the calcination temperature, J. Porous. Mater. 2 (1996) 291–297, https://doi.org/10.1007/BF00489810.
[89] T.M. Rossi, J.C. Campos, M.M.V.M. Souza, An evaluation of calcined hydrocalumite as carbon dioxide adsorbent using thermogravimetric analysis, Appl. Clay Sci. 182 (2019) 105252, https://doi.org/10.1016/j.clay.2019.105252.
[90] A. Takagaki, K. Iwatani, S. Nishimura, K. Ebitani, Synthesis of glycerol carbonate from glycerol and dialkyl carbonates using hydrotalcite as a reusable heterogeneous base catalyst, Green Chem. 12 (4) (2010) 578, https://doi.org/10.1039/b925404H.